scientific reports

OPEN

Powdered and beaded sawdust materials modified iron (III) oxide-hydroxide for adsorption of lead (II) ion and reactive blue 4 dye

Pornsawai Praipipat [1,2]✉, Pimploy Ngamsurach[1,2], Sichon Kosumphan[1] & Jirasak Mokkarat[1]

The problems of lead and reactive blue 4 (RB4) dye contamination in wastewater are concerns because of their toxicities to aquatic life and water quality, so lead and RB4 dye removals are recommended to remove from wastewater before discharging. Sawdust powder (SP), sawdust powder doped iron (III) oxide-hydroxide (SPF), sawdust beads (SPB), and sawdust powder doped iron (III) oxide-hydroxide beads (SPFB) were synthesized and characterized with various techniques, and their lead or RB4 dye removal efficiencies were investigated by batch experiments, adsorption isotherms, kinetics, and desorption experiments. SPFB demonstrated higher specific surface area (11.020 m^2 g^{-1}) and smaller pore size (3.937 nm) than other materials. SP and SPF were irregular shapes with heterogeneous structures whereas SPB and SPFB had spherical shapes with coarse surfaces. Calcium (Ca) and oxygen (O) were found in all materials whereas iron (Fe) was only found in SPF and SPFB. O–H, C–H, C=C, and C–O were detected in all materials. Their lead removal efficiencies of all materials were higher than 82%, and RB4 dye removal efficiencies of SPB and SPFB were higher than 87%. Therefore, adding iron (III) oxide-hydroxide and changing material form helped to improve material efficiencies for lead or RB4 dye adsorption. SP and SPB corresponded to Langmuir model related to a physical adsorption process whereas SPF and SPFB corresponded to the Freundlich model correlated to a chemisorption process. All materials corresponded to a pseudo-second-order kinetic model relating to the chemical adsorption process. All materials could be reused more than 5 cycles with high lead removal of 63%, and SPB and SPFB also could be reused more than 5 cycles for high RB4 dye removal of 72%. Therefore, SPFB was a potential material to apply for lead or RB4 dye removal in industrial applications.

Water pollutions from heavy metals or dye contaminations create many problems with water quality, toxicity to aquatic life and the environment, a decrease of oxygen in water sources, an obstacle to sunlight for photosynthesis, and persistent, accumulation, and transport through the food chain. In addition, they also create many human health effects of dysfunctions in human systems such as the brain, blood, reproduction, digestive, and respiratory and cause cancers[1]. Especially, lead (Pb) is a toxic heavy metal with concern its toxicity with persistent and bioaccumulation. A reactive blue 4 (RB4) dye is popularly used in the textile industry because it offers long-lasting color in the fabric. However, if it is released into the environment without treatment, it affects aquatic life and the environment as mentioned above. The sources of releasing lead or RB4 dye are various industries of battery, electronic, paint, dye, plastic, and textile using them in their manufacturing processes[2,3], so their wastewater might consist of lead or RB4 dye. As a result, wastewater with lead or dye contamination is required for a treatment to be below water quality standards for safety purposes.

Many methods of chemical precipitation, coagulation-flocculation, electrochemical, ion exchange, and reverse osmosis are used for eliminating heavy metals or dyes in wastewater; however, they have limitations of incompletely heavy metal removals, complicated operations with expensive costs including creating toxic sludges with requiring disposals[4]. As a result, many studies attempted to find an alternative method with an effective and

[1]Department of Environmental Science, Khon Kaen University, Khon Kaen 40002, Thailand. [2]Environmental Applications of Recycled and Natural Materials (EARN) Laboratory, Khon Kaen University, Khon Kaen 40002, Thailand. ✉email: pornprai@kku.ac.th

environmentally friendly instead of them. An adsorption method is a good method to solve the above problems because this method offers high heavy metal and dye removals, suitable cost, simple operation, and creating low sludge volume[5]. In addition, various available choices of adsorbents of this method are a good option for a user with considering which adsorbent is good for removing a target pollutant by using the considering criteria of available adsorbent in that area, water quality after treatment, and budget. Several adsorbents are used for eliminating specific a target metal or dye ion in wastewater such as activated carbon, chitosan, zeolite, fruit peels, and wastes of agriculture, food, and industrial; however, this study will focus on various wastes as low-cost adsorbents used for improving water quality along with reducing waste volumes in terms of waste management. The elimination of heavy metals or dyes from wastewater from various wastes is demonstrated in Table 1. Among those adsorbents, sawdust is a good offer because it has good chemical properties of cellulose, hemicellulose, lignin, pectin, hydroxyl, and carboxyl groups for good lead or RB4 dye adsorption in wastewater. Furthermore, using sawdust can reduce a huge of sawmill factory waste and help to manage the problem of waste disposal along with improving water quality by using sawdust as an adsorbent material. Although sawdust has good chemical properties for removing lead or RB4 dye, the material improvement method needs to study for increasing lead or RB4 dye removal efficiencies in case of high-strength lead or RB4 dye concentration in industrial applications.

For material modifications, many previous studies have been reported for using a variety of metal oxides of iron (II or III) oxide (Fe_4O_3 or Fe_2O_3), zinc oxide (ZnO), titanium dioxide (TiO_2), aluminum oxide (Al_2O_3), tin (IV) oxide (SnO_2), and magnesium oxide (MgO) to increase surface area and pore volume of adsorbents offering to increase lead or RB4 dye removal efficiency[6–8]. The modified materials of sugarcane bagasse with Fe_2O_3, sawdust with ZnO, and lemon peels with iron (III) oxide-hydroxide have been used for lead removal[8–10], and the

Adsorbent materials	Heavy metal/dye	Dose	Contact time	Temperature (°C)	pH	Concentration (mg L^{-1})	Removal efficiency (%)	References
Paddy husk (Biochar)	Lead (Pb^{2+})	0.1 g	24 h	25	6	10	99.00	[15]
Paddy husk (Biochar)	Copper (Cu^{2+})	0.1 g	24 h	25	6	10	99.00	[15]
Paddy husk (Biochar)	Zinc (Zn^{2+})	0.1 g	24 h	25	7.5	10	99.00	[15]
Sawdust (Biochar)	Lead (Pb^{2+})	0.1 g	24 h	25	6	10	99.00	[15]
Sawdust (Biochar)	Copper (Cu^{2+})	0.1 g	24 h	25	6	10	99.00	[15]
Sawdust (Biochar)	Zinc (Zn^{2+})	0.1 g	24 h	25	7.5	10	99.00	[15]
Pine wood sawdust modified with maleic acid	Cadmium (Cd^{2+})	0.3 g L^{-1}	2 h	130	6	130	–	[16]
Bagasse	Lead (Pb^{2+})	1 g	2 h	–	5.5	100	74.40–80.00	[17]
Bagasse	Cadmium (Cd^{2+})	1 g	2 h	–	5.5	100	66.70–82.35	[17]
Eggshell	Lead (Pb^{2+})	1 g	2 h	–	5.5	100	99.55	[17]
Eggshell	Cadmium (Cd^{2+})	1 g	2 h	–	5.5	100	53–75	[17]
Lemon peel powder	Lead (Pb^{2+})	4 g	6 h	25	5	100	86.00	[18]
Lemon peel beads	Lead (Pb^{2+})	5 g	6 h	25	5	100	97.00	[18]
Melon peels	Lead (Pb^{2+})	1.5 g L^{-1}	1 h	30	7	10	98.50	[19]
Melon peels	Copper (Cu^{2+})	1.5 g L^{-1}	1 h	30	6	10	99.10	[19]
Melon peels	Cadmium (Cd^{2+})	1.5 g L^{-1}	1 h	30	6	10	99.20	[19]
Cordia trichotoma sawdust	Crystal violet	0.8 g L^{-1}	2 h	55	7.5	200	82.22	[20]
Potato peels	Cibacron blue P3R	2 g L^{-1}	3 h	25	2.2	30	76.41	[21]
Potato peels modified with phosphoric acid	Cibacron blue P3R	2 g L^{-1}	3 h	25	2.2	30	88.60	[21]
Potato peels calcined at 800 °C	Cibacron blue P3R	0.6 g L^{-1}	3 h	25	2.2	30	94.00	[21]
Banana peels	Reactive black 5	0.3 g	24 h	25	3	300	–	[22]
Banana peels	Cong red	0.3 g	24 h	25	3	300	–	[22]
Fava bean peels	Methylene blue	5 g L^{-1}	24 h	27	5.8	50	70.00–80.00	[23]
Clinoptilolite modified with Fe_3O_4	Basic violet 16	0.5 g L^{-1}	45 min	–	7	25	99.00	[24]
Activated carbon modified with Fe_3O_4	Reactive blue 19	1 g L^{-1}	45 min	–	3	100	93.22	[25]
Activated carbon modified with zinc oxide	Reactive blue 19	1.5 g L^{-1}	45 min	–	3	100	97.36	[26]
Activated carbon modified with zinc oxide	Reactive black 5	1.5 g L^{-1}	45 min	–	3	100	73.36	[26]
Walnut peel activated carbon modified with zinc oxide	Acid blue 113	0.5 g L^{-1}	15 min	–	3	100	98.20	[27]
Walnut peel activated carbon modified with zinc oxide	Eosin Y	1 g L^{-1}	30 min	–	3	100	95.11	[28]
Walnut peel activated carbon modified with zinc oxide	Erythrosine B	1 g L^{-1}	30 min	–	3	100	98.31	[28]

Table 1. The elimination of heavy metals or dyes from wastewater from various industrial wastes.

modifications of rice bran with SnO_2/Fe_3O_4, bagasse with zinc oxide, and lemon peels beads with iron (III) oxide-hydroxide have been applied for removing RB4 dye[11–13]. Moreover, the stability of the material is another point for applying industrial application, so the changing of material form from a powder form to a bead form in many studies has also been reported with supporting the increase of heavy metal or dye removal efficiencies[6–8,12–14]. Therefore, this study attempts to synthesize sawdust materials modified with iron (III) oxide-hydroxide in powder and bead materials, compare their lead or RB4 dye removal efficiencies through batch experiments, and verify whether adding metal oxide or changing form helped to improve a material efficiency for lead or RB4 adsorption.

The study aimed to synthesize four types of adsorbent materials which were sawdust powder (SP), sawdust powder doped iron (III) oxide-hydroxide (SPF), sawdust beads (SPB), and sawdust powder doped iron (III) oxide-hydroxide beads (SPFB). Several characterized techniques of Brunauer–Emmett–Teller (BET), field emission scanning electron microscopy and focus ion beam (FESEM-FIB) with energy dispersive X-ray spectrometer (EDX), and Fourier transform infrared spectroscopy (FT-IR) were used to investigate their specific surface area, pore volume, pore size, surface morphologies, chemical compositions, and chemical functional groups. Lead or RB4 dye removal efficiencies of SP, SPF, SPB, and SPFB were examined by batch experiments with varying doses, contact time, temperature, pH, and concentration. Moreover, linear and nonlinear adsorption isotherms of Langmuir, Freundlich, Temkin, and Dubinin–Radushkevich models and kinetics of pseudo-first-kinetic, pseudo-second-kinetic, Elovich, and intraparticle diffusion models were used for investigating their lead or RB4 dye adsorption patterns and mechanisms. Finally, the desorption experiments were also investigated for confirming the reusability of sawdust materials for lead or RB4 dye adsorption.

Result and discussion

The physical characteristics of sawdust materials.

The physical characteristics of sawdust powder (SP), sawdust powder doped iron (III) oxide-hydroxide (SPF), sawdust beads (SPB), and sawdust powder doped iron (III) oxide-hydroxide beads (SPFB) are demonstrated in Fig. 1a–d. SP had light brown color powder whereas SPF had brown color powder shown in Fig. 1a,b. SPF had brown color beads while SPFB had dark brown color beads demonstrated in Fig. 1c,d.
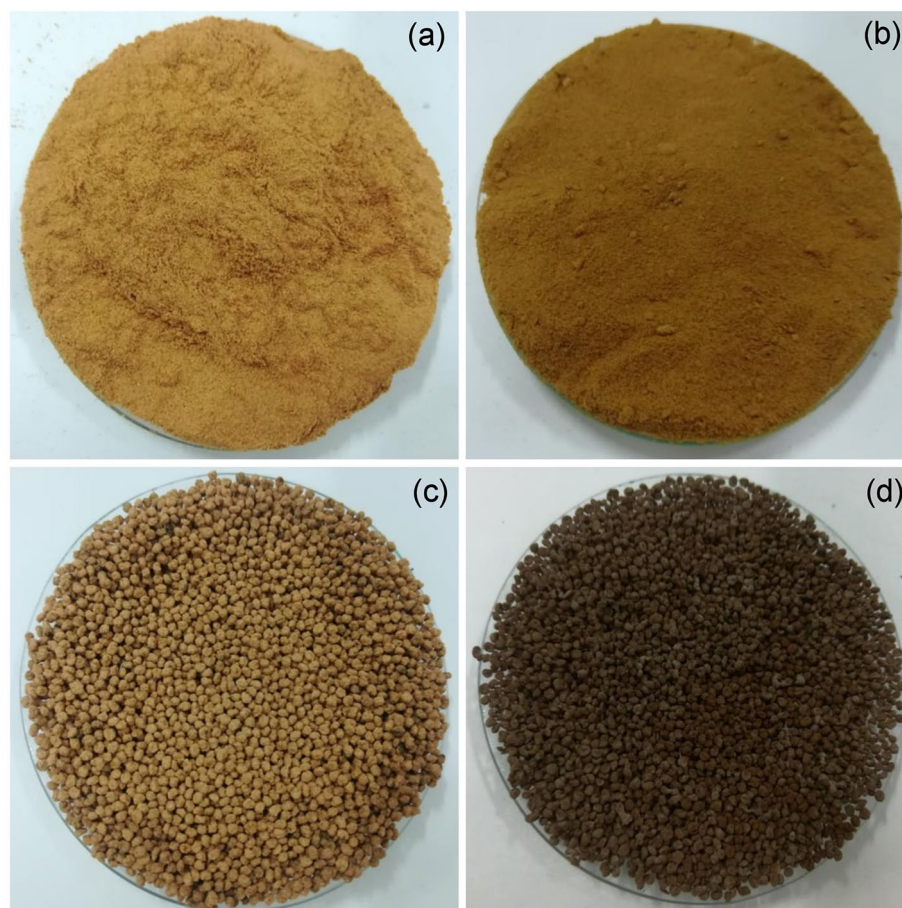

Figure 1. The physical characteristics of (**a**) sawdust powder (SP), (**b**) sawdust powder doped iron (III) oxide-hydroxide (SPF), (**c**) sawdust beads (SPB), and (**d**) sawdust powder doped iron (III) oxide-hydroxide beads (SPFB).

Characterizations of sawdust materials. *BET analysis.* The specific surface area, pore volume, and pore diameter size of sawdust powder (SP), sawdust powder doped iron (III) oxide-hydroxide (SPF), sawdust beads (SPB), and sawdust powder doped iron (III) oxide-hydroxide beads (SPFB) determined by the Brunauer–Emmet and Teller technique (BET) with N_2 adsorption–desorption isotherm at 77.3 K and degas temperature of 80 °C for 6 h, and the results of specific surface area and pore volume by Brunauer–Emmett–Teller (BET) and pore size by Barrett–Joyner–Halenda (BJH) method are reported in Table 2.

For the specific surface area of SP, SPF, SPB, and SPFB, they were 0.328, 1.551, 1.960, and 11.020 $m^2 g^{-1}$, respectively which SPFB demonstrated the highest specific surface area than other materials. In addition, their pore volumes were 0.075, 0.356, 0.250, and 2.532 $cm^3 g^{-1}$, respectively, and their pore diameter sizes were 4.256, 3.940, 4.068, and 3.937 nm, respectively. As a result, the addition of iron (III) oxide-hydroxide into sawdust materials (SPF and SPFB) increased the specific surface area and pore volume while the pore diameter size was decreased. In addition, all three parameters increased from changing material form from SP to SPB. Since their pore size was in a range of 2–50 nm, they were classified as mesoporous by the classification of International Union of Pure and Applied Chemistry (IUPAC)[35].

For the BET comparison, SP had a lower specific surface area than all studies reported in Table 2 whereas SPF, SPB, and SPFB had higher values than the studies of Chen et al. and Houshangi et al.[29,34]. The studies of Chen et al. and Houshangi et al. had been reported that the modifications of sawdust materials by sodium hydroxide (NaOH) or triethanolamine ($C_6H_{15}NO_3$) or iron dioxide (Fe_2O_4) helped to increase specific surface area similar to this study[29,34].

FESEM-FIB analysis. The surface morphologies of sawdust powder (SP), sawdust powder doped iron (III) oxide-hydroxide (SPF), sawdust beads (SPB), and sawdust powder doped iron (III) oxide-hydroxide beads (SPFB) by FESEM-FIB analysis at 500× magnification with 400 µm for a surface and at 100× magnification with 1 mm for a bead illustrated in Fig. 2a–f. SP and SPF were irregular shapes with heterogeneous fiber structures demonstrated in Fig. 2a,b similar reported of sawdust morphologies by other studies[36,37]. For SPB, it had a spherical shape with a coarse surface at 100× magnification with 1 mm shown in Fig. 2c, and its surface was a rough surface when zoomed at 500× magnification with 400 µm demonstrated in Fig. 2d. Finally, SPFB had a spherical shape with a coarse surface at 100× magnification of 1 mm shown in Fig. 2e, and its surface was an irregular shape with the heterogenous surface when zoomed at 500× magnification with 400 µm illustrated in Fig. 2f.

EDX analysis. The chemical compositions of sawdust powder (SP), sawdust powder doped iron (III) oxide-hydroxide (SPF), sawdust beads (SPB), and sawdust powder doped iron (III) oxide-hydroxide beads (SPFB) were analyzed by using EDX analysis represented in Table 3, and the elemental mapping of SP, SPF, SPB, and SPFB demonstrated in Fig. 3a–d which showed the dispersions of chemical elements of each material on the surface. Two main chemical components of carbon (C) and oxygen (O) were found in all materials while copper (Cu) was only found in powder materials of SP and SPF. For calcium (Ca), it was detected in SPB and SPFB. For sodium (Na) and chloride (Cl), they were observed in all materials except SP. In addition, iron (Fe) was found in the materials with the addition of iron (III) oxide-hydroxide which were SPF and SPFB to confirm the successful adding Fe into SP and SPB. For SP and SPF, the mass percentages by weight of C and O were decreased when iron (III) oxide-hydroxide was added to SP whereas Cu was increased. Moreover, Na, Cl, and Fe were detected in SPF which might be from using chemicals in a process of adding iron (III) oxide-hydroxide by ferric chlo-

Adsorbent materials	Surface area ($m^2 g^{-1}$)	Pore volume ($cm^3 g^{-1}$)	Pore diameter size (nm)	References
Sawdust	0.697	–	11.399	[29]
Sawdust	1.090	–	–	[30]
Palm date sawdust	1.360	–	0.500	[31]
Pine sawdust biochar	13.080	0.010	1.320	[32]
Sawdust modified by sodium hydroxide and triethanolamine	0.969	–	24.485	[29]
Wheat bran sawdust modified by Fe_3O_4	74.250	0.119	6.422	[33]
Unmodified sawdust	–	0.004	–	[34]
Unmodified sawdust mixed $CoFe_2O_4$	18.083	0.098	26.603	[34]
Unmodified sawdust mixed $NiFe_2O_4$	19.649	0.085	17.202	[34]
Modified sawdust	0.230	0.006	103.790	[34]
Modified sawdust mixed $CoFe_2O_4$	18.077	0.083	18.363	[34]
Modified sawdust mixed $NiFe_2O_4$	91.736	0.250	10.901	[34]
SP	0.328	0.075	4.256	This study
SPF	1.551	0.356	3.940	This study
SPB	0.960	0.250	4.068	This study
SPFB	11.020	2.532	3.937	This study

Table 2. The specific surface area, pore volumes, and pore size of sawdust materials with comparing other studies.
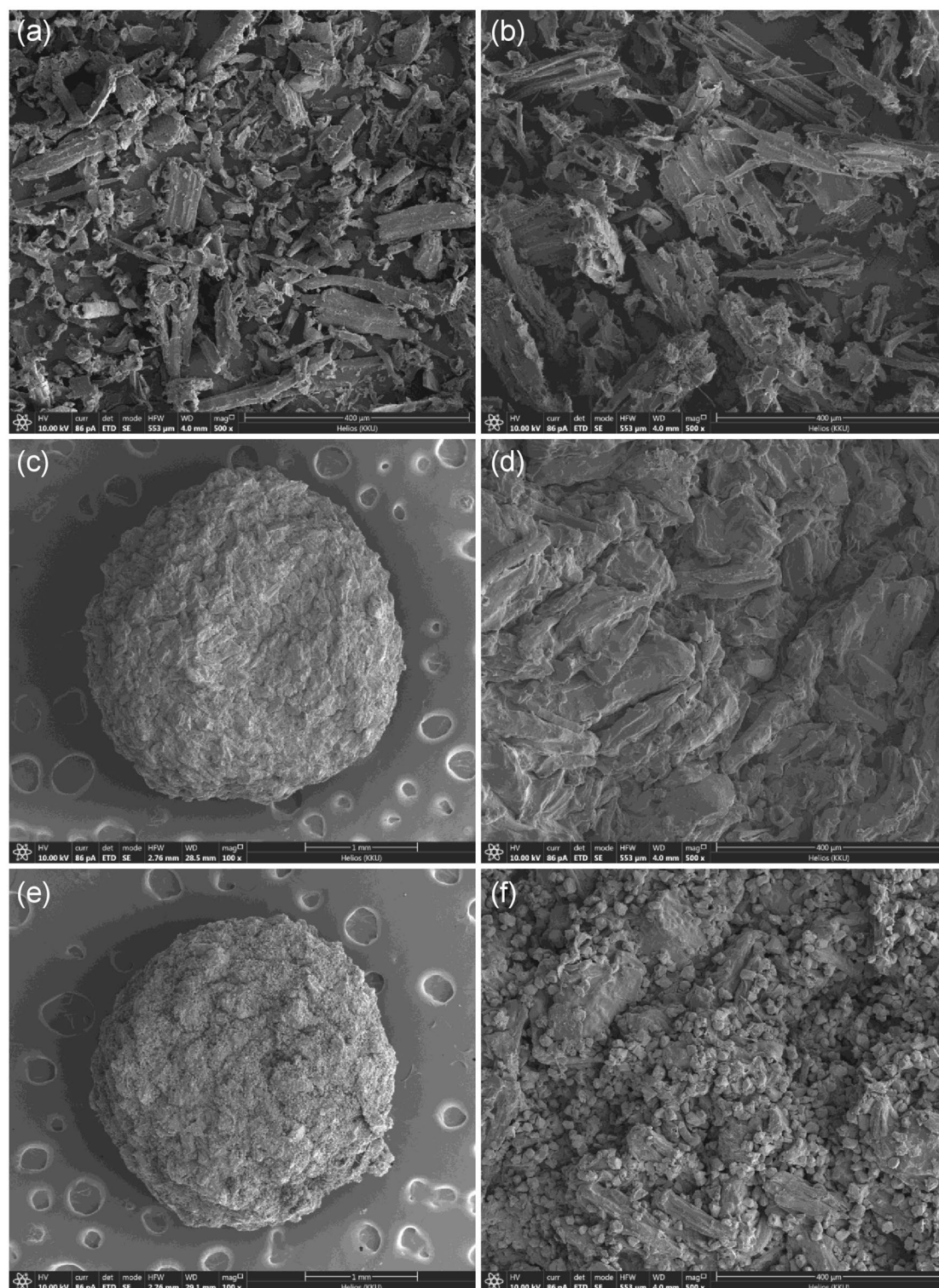
Figure 2. The surface morphologies of (**a**) sawdust powder (SP), (**b**) sawdust powder doped iron (III) oxide-hydroxide (SPF), (**c,d**) sawdust beads (SPB), and (**e,f**) sawdust powder doped iron (III) oxide-hydroxide beads (SPFB).

ride hexahydrate ($FeCl_3 \cdot 6H_2O$) and sodium hydroxide (NaOH) for synthesizing SPF. For SP and SPB, the mass percentage by weight of C was deceased while O was increased after changing the material to a bead form. In addition, the mass percentages by weight of Ca, Na, and Cl were also detected in SPB by using sodium alginate ($NaC_6H_7O_6$) and calcium chloride ($CaCl_2$) in a bead formation. For SPF and SPFB, the mass percentages by weight of C, O, and Na were decreased. While the mass percentages by weight of Ca, Cl, and Fe were increased when SPF was changed to a bead form. The increases of Ca and Cl might be from using chemicals of $CaCl_2$ in a

Chemical composition (%wt)	Sawdust materials			
	SP	SPF	SPB	SPFB
C	59.6	48.2	51.7	32.6
O	39.0	38.1	40.5	31.0
Cu	1.4	1.5	–	–
Ca	–	–	5.1	23.2
Na	–	8.4	0.5	0.7
Cl	–	0.2	2.2	1.3
Fe	–	3.6	–	11.3

Table 3. The chemical compositions of sawdust powder (SP), sawdust powder doped iron (III) oxide-hydroxide (SPF), sawdust beads (SPB), and sawdust powder doped iron (III) oxide-hydroxide beads (SPFB) in the percentages by weight.

process of a bead formation similar to SPB. Therefore, the addition of iron (III) oxide-hydroxide and the changing material form affected the increases of Ca, Na, Cl, and Fe contents in sawdust materials.

FT-IR analysis. The chemical functional groups of sawdust powder (SP), sawdust powder doped iron (III) oxide-hydroxide (SPF), sawdust beads (SPB), and sawdust powder doped iron (III) oxide-hydroxide beads (SPFB) were examined by FT-IR analysis, and their FT-IR spectra are demonstrated in Fig. 4a–d. Four main function groups of O–H, C–H, C=C, and C–O were detected in all materials. In addition, the carboxyl group of sodium alginate (–COOH) was found in bead materials (SPB and SPFB)[38], and Fe–O was observed in materials with adding iron (III) oxide-hydroxide (SPF and SPFB)[39]. O–H represented the stretching of hydroxyl, alcohol, and phenolic groups of cellulose fiber, lignin, and pectin, and C–H demonstrated the stretching of a methyl group (–CH$_2$) in cellulose and hemicellulose[40]. C=C referred to the stretching of aromatic rings corresponding to the lignin, and C–O was the stretching of alcohol and carboxylic acid of lignin and hemicellulose[41]. For SP, it detected the stretching of O–H at 3322.83 cm^{-1}, stretching of C–H at 2918.28 cm^{-1}, stretching of C=C at 1666.59 cm^{-1}, and stretching of C–O at 1245.34 and 1030.31 cm^{-1} illustrated in Fig. 4a. For SPF, it observed the stretching of O–H at 3325.99 cm^{-1}, stretching of C–H at 2916.52 cm^{-1}, C=C at 1664.48 cm^{-1}, stretching of C–O at 1262.29 and 1028.88 cm^{-1}, and Fe–O at 847.36 cm^{-1} shown in Fig. 4b. For SPB, it identified the stretching of O–H at 3323.08 cm^{-1}, C–H at 2910.48 cm^{-1}, C=C at 1664.90 cm^{-1}, stretching of C–O at 1249.35 and 1021.42 cm^{-1}, and –COOH at 1419.56 cm^{-1} shown in Fig. 4c. For SPFB, it found the stretching of O–H at 3323.68 cm^{-1}, stretching of C–H at 2919.56 cm^{-1}, C=C at 1664.33 cm^{-1}, stretching of C–O at 1262.71 and 1024.87 cm^{-1}, –COOH at 1421.49 cm^{-1}, and Fe–O at 813.34 cm^{-1} shown in Fig. 4d.

Batch adsorption experiments for lead and RB4 dye removals. *The effect of dose.* For lead removal, five different doses from 0.5 to 3 g were used for investigating the dose effect of lead adsorption by sawdust powder (SP), sawdust powder doped iron (III) oxide-hydroxide (SPF), sawdust beads (SPB), and sawdust powder doped iron (III) oxide-hydroxide beads (SPFB), and the results are demonstrated in Fig. 5a. The control condition was the lead concentration of 50 mg L^{-1}, a sample volume of 200 mL, a contact time of 6 h, pH 5, a temperature of 25 °C, and a shaking speed of 200 rpm. Lead removal efficiencies of all materials were increased with the increase of material dose which might be from the increase of active sites of materials[7]. Their highest lead removal efficiencies were 85.12%, 96.11%, 89.57%, and 100% at 2 g, 1 g, 1.5 g, and 0.5 g for SP, SPF, SPB, and SPFB, respectively. Therefore, they were optimum doses of sawdust materials that were used for studying the contact time effect.

For RB4 dye removal, six different doses from 0.5 to 3 g were used for investigating the dose effect of RB4 dye adsorption by sawdust beads (SPB) and sawdust powder doped iron (III) oxide-hydroxide beads (SPFB), and the results are demonstrated in Fig. 5b. The control condition was the RB4 dye concentration of 50 mg L^{-1}, a sample volume of 200 mL, a contact time of 12 h, pH 7, a temperature of 60 °C, and a shaking speed of 150 rpm. RB4 dye removal efficiencies of all materials were increased with the increase of material dose which might be from the increase of active sites of materials[12]. The highest RB4 dye removal efficiency of SPB was found at 3 g with 89.65% while the highest RB4 dye removal efficiency of SPFB was found at 1.5 g with 94.10%. Therefore, they were the optimum dosages of sawdust materials that were used for studying the contact time effect.

The effect of contact time. For lead removal, the different contact times from 1 to 6 h were used for studying the contact time effect on lead adsorptions by sawdust powder (SP), sawdust powder doped iron (III) oxide-hydroxide (SPF), sawdust beads (SPB), and sawdust powder doped iron (III) oxide-hydroxide beads (SPFB), and the results are demonstrated in Fig. 5c. The control condition was the lead concentration of 50 mg L^{-1}, a sample volume of 200 mL, pH 5, a temperature of 25 °C, a shaking speed of 200 rpm, and the optimum dose of 2 g (SP) or 1 g (SPF) or 1.5 g (SPB) or 0.5 g (SPFB). Lead removal efficiencies of all materials were increased with the increase of contact time similar to the dose effect. Their highest lead removal efficiencies were 86.74%, 97.58%, 90.12%, and 100% at 5 h, 3 h, 4 h, and 2 h for SP, SPF, SPB, and SPFB, respectively. Therefore, they were the optimum contact time of sawdust materials that were used for studying the pH effect.
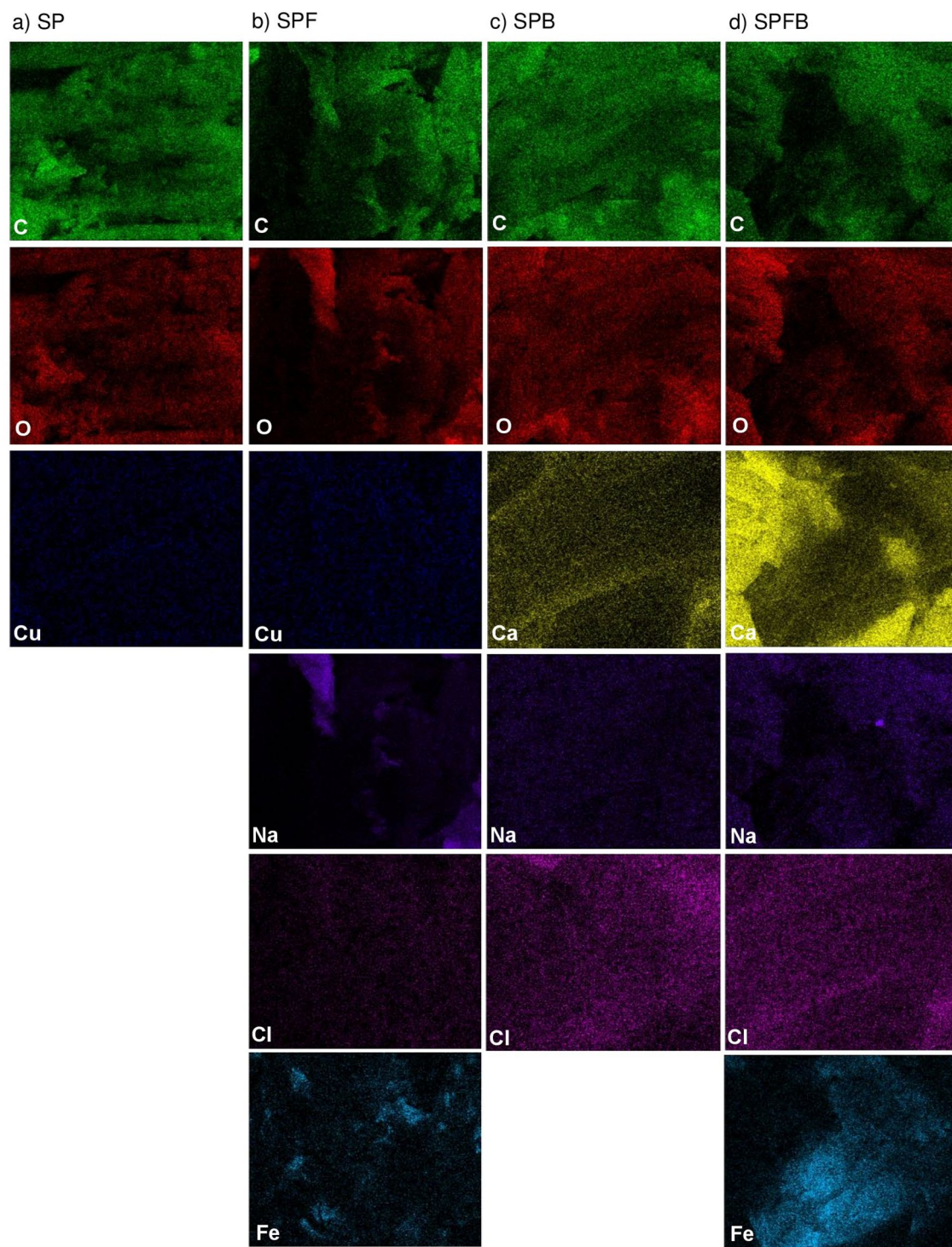
Figure 3. The elemental mapping of (**a**) sawdust powder (SP), (**b**) sawdust powder doped iron (III) oxide-hydroxide (SPF), (**c**) sawdust beads (SPB), and (**d**) sawdust powder doped iron (III) oxide-hydroxide beads (SPFB) on the surface.

For RB4 dye removal, the different contact times from 3 to 18 h were used for studying the contact time effect on RB4 dye adsorptions by sawdust beads (SPB) and sawdust powder doped iron (III) oxide-hydroxide beads (SPFB), and the results are demonstrated in Fig. 5d. The control condition was the RB4 dye concentration of 50 mg L^{-1}, a sample volume of 200 mL, pH 7, a temperature of 60 °C, a shaking speed of 150 rpm, and the optimum dose 3 g (SPB) or 1.5 g (SPFB). RB4 dye removal efficiencies of all materials were increased with the increase of contact time similar to the dose effect. Their highest RB4 dye removal efficiencies were found at 12 h
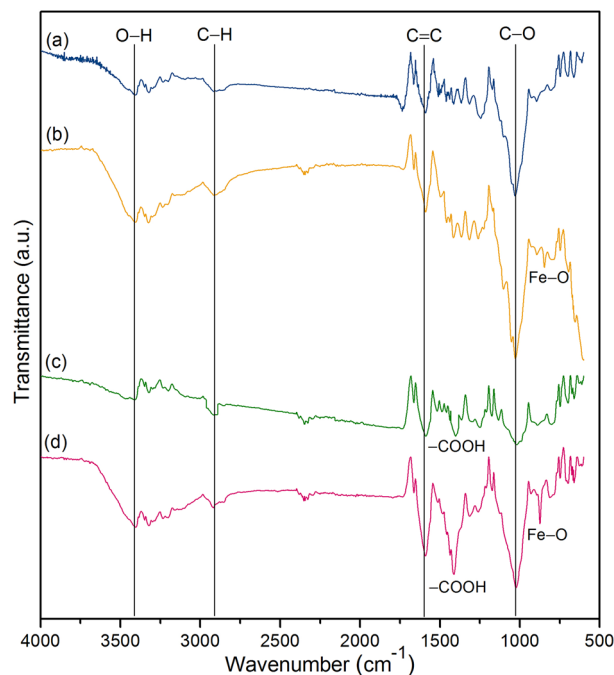
Figure 4. FT-IR spectra of (**a**) sawdust powder (SP), (**b**) sawdust powder doped iron (III) oxide-hydroxide (SPF), (**c**) sawdust beads (SPB), and (**d**) sawdust powder doped iron (III) oxide-hydroxide beads (SPFB).

with 88.15% for SPB and 9 h with 93.76% for SPFB. Therefore, they were the optimum contact times of sawdust materials that were used for studying the pH effect.

The effect of temperature effect. Only dye removal investigated the effect of temperature whether the changing temperature affects RB4 dye removal by sawdust beads (SPB) and sawdust powder doped iron (III) oxide-hydroxide beads (SPFB). The different temperatures from 40 to 80 °C were used for studying the temperature effect on RB4 dye adsorptions by sawdust materials, and the results are demonstrated in Fig. 5f. The control condition was the RB4 dye concentration of 50 mg L^{-1}, a sample volume of 200 mL, pH 7, a shaking speed of 150 rpm, and the optimum dose of 3 g (SPB) or 1.5 g (SPFB) and contact time of 12 h (SPB) or 9 h (SPFB). RB4 dye removal efficiencies of all materials were decreased with the increase of temperature, and the highest RB4 dye removal efficiencies were at a temperature of 40 °C with 87.78% for SPB and 30 °C with 95.12% for SPFB. Therefore, they were the optimum temperatures of sawdust materials that were used for studying the pH effect.

The effect of pH. For lead removal, the effect of pH was studied by varying pH values of 1, 3, 5, 7, 9, and 11 represented the acid, neutral, and base conditions on lead adsorptions by sawdust powder (SP), sawdust powder doped iron (III) oxide-hydroxide (SPF), sawdust beads (SPB), and sawdust powder doped iron (III) oxide-hydroxide beads (SPFB), and the results are demonstrated in Fig. 5e. The control condition was the lead concentration of 50 mg L^{-1}, a sample volume of 200 mL, a temperature of 25 °C, a shaking speed of 200 rpm, and the optimum dose of 2 g (SP) or 1 g (SPF) or 1.5 g (SPB) or 0.5 g (SPFB) and contact time of 5 h (SP) or 3 h (SPF) or 4 h (SPB) or 2 h (SPFB). Lead removal efficiencies of all materials were increased with the increase of pH values from 1 to 7, then they were decreased. Their highest lead removal efficiencies of all materials were found at pH 5 with lead removal at 86.21%, 98.15%, 91.45%, and 100% for SP, SPF, SPB, and SPFB, respectively which corresponded to other previous studies reported the highest lead removal efficiency at pH > 4[7,8,18]. Therefore, pH 5 was the optimum pH of sawdust materials that were used for studying the concentration effect.

For RB4 dye removal, the effect of pH was studied by varying pH values of 1, 3, 5, 7, 9, and 11 represented the acid, neutral, and base conditions on RB4 dye adsorptions by sawdust beads (SPB) and sawdust powder doped iron (III) oxide-hydroxide beads (SPFB), and the results are demonstrated in Fig. 5h. The control condition was the RB4 dye concentration of 50 mg L^{-1}, a sample volume of 200 mL, a shaking speed of 150 rpm, and the optimum dose 3 g (SPB) or 1.5 g (SPFB), contact time of 12 h (SPB) or 9 h (SPFB), and temperature of 40 °C (SPB) or 30 °C (SPFB). RB4 dye removal efficiencies of all materials were increased with the increase of pH values from 1 to 3, then they were decreased. Their highest RB4 dye removal efficiencies of all materials were found at pH 3 with RB4 dye removal at 89.12% and 95.96% for SPB and SPFB which corresponded to other previous studies reported the highest RB4 dye removal efficiency found at acidic conditions[6,14]. Therefore, pH 3 was the optimum pH of sawdust materials that were used for studying the concentration effect.

The effect of concentration. For lead removal, lead concentrations of 30–70 mg L^{-1} were used to investigate the concentration effect on lead adsorptions by sawdust powder (SP), sawdust powder doped iron (III) oxide-
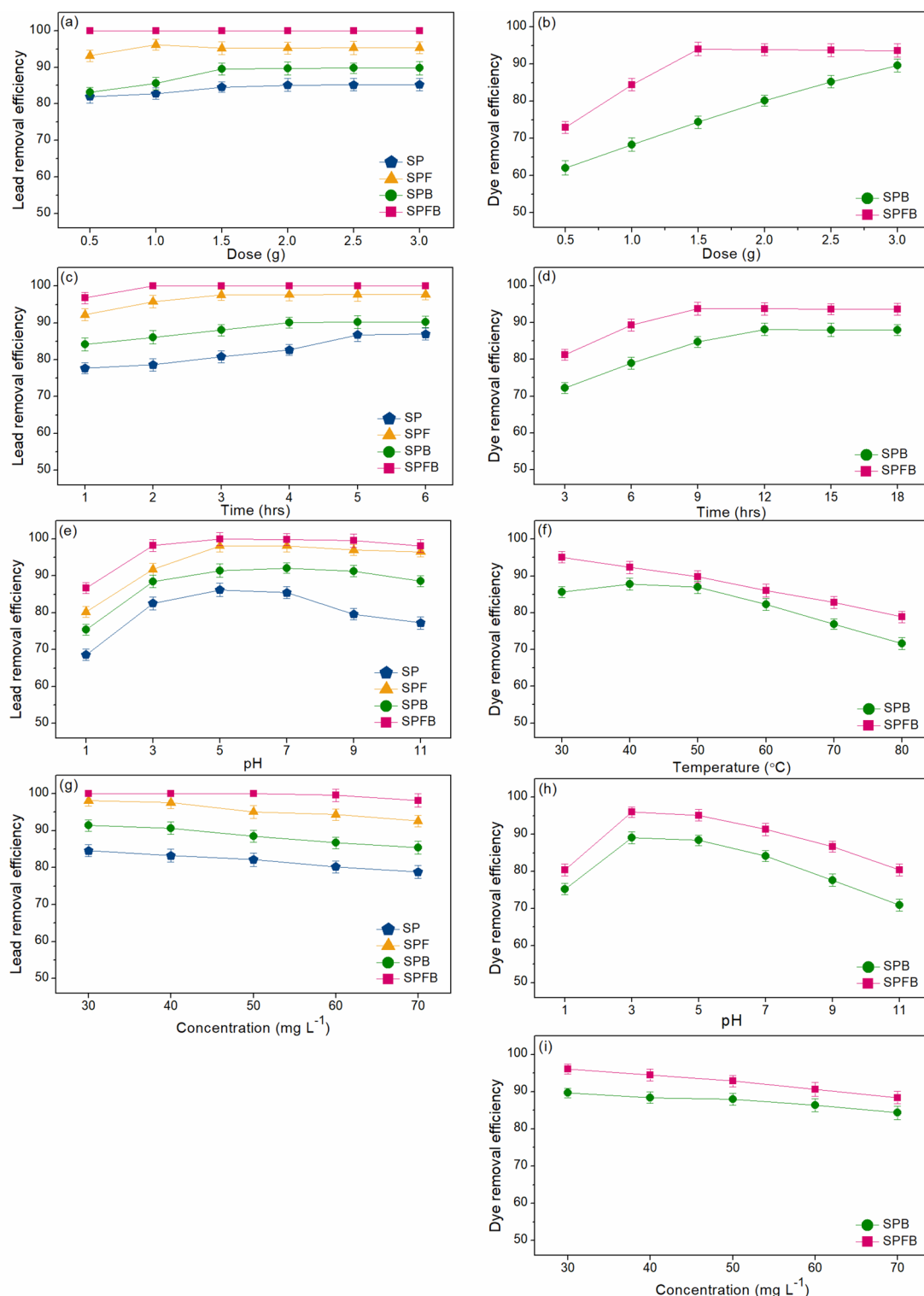
Figure 5. Batch experiments for lead and RB4 dye removals on the effects of (**a,b**) dose, (**c,d**) contact time, (**f**) temperature, (**e,h**) pH, and (**g,i**) concentration of sawdust powder (SP), sawdust powder doped iron (III) oxide-hydroxide (SPF), sawdust beads (SPB), and sawdust powder doped iron (III) oxide-hydroxide beads (SPFB).

hydroxide (SPF), sawdust beads (SPB), and sawdust powder doped iron (III) oxide-hydroxide beads (SPFB), and the results are demonstrated in Fig. 5g. The control condition was a sample volume of 200 mL, a temperature of 25 °C, a shaking speed of 200 rpm, and the optimum dose of 2 g (SP) or 1 g (SPF) or 1.5 g (SPB) or 0.5 g (SPFB) and contact time of 5 h (SP) or 3 h (SPF) or 4 h (SPB) or 2 h (SPFB), and pH of 5. Lead removal efficiencies of all materials were decreased with the increase of concentration because of the decreasing available active sites for adsorbing lead ions[7]. Lead removal efficiencies from 30 to 70 mg L^{-1} of SP, SPF, SPB, and SPFB were 78.82–

84.56%, 92.57–98.12%, 85.41–91.39%, and 97.15–100%, respectively. For the lead concentration of 50 mg L^{-1}, lead removal efficiencies of SP, SPF, SPB, and SPFB were 82.14%, 95.06%, 88.45%, and 100%, respectively, and SPFB demonstrated the highest lead removal efficiency of other materials.

For RB4 dye removal, RB4 dye concentrations of 30–70 mg L^{-1} were used to investigate the concentration effect on RB4 dye adsorptions by sawdust beads (SPB) and sawdust powder doped iron (III) oxide-hydroxide beads (SPFB), and the results are demonstrated in Fig. 5i. The control condition was a sample volume of 150 mL, and the optimum dose of 3 g (SPB) or 1.5 g (SPFB), contact time of 12 h (SPB) or 9 h (SPFB), temperature of 40 °C (SPB) or 30 °C (SPFB), and pH of 3. RB4 dye removal efficiencies of all materials were decreased with the increase of concentration because RB4 dye ions were more than the available active sites of sawdust materials similar to the report by other studies[12,14]. RB4 dye removal efficiencies from 30 to 70 mg L^{-1} of SPB and SPFB were 84.35–89.65% and 88.43–96.12%. For the RB4 dye concentration of 50 mg L^{-1}, RB4 dye removal efficiencies of SPB and SPFB were 87.96% and 92.84%, and SPFB demonstrated the highest RB4 dye removal efficiency of other materials.

In conclusion of lead removal, 2 g, 5 h, pH 5, 50 mg L^{-1}, 1 g, 3 h, pH 5, 50 mg L^{-1}, 1.5 g, 4 h, pH 5, 50 mg L^{-1}, and 0.5 g, 2 h, pH 5, 50 mg L^{-1} were the optimum conditions in dose, contact time, pH, and concentration of SP, SPF, SPB, and SPFB, respectively, and they could be arranged in order from high to low of SPFB > SPF > SPB > SP. As a result, both changing material form and adding iron (III) oxide-hydroxide helped to improve material efficiency for lead adsorption.

In conclusion of RB4 dye removal, 3 g, 12 h, 40 °C, pH 3, 50 mg L^{-1} and 1.5 g, 9 h, 30 °C, pH 3, 50 mg L^{-1} were the optimum conditions in dose, contact time, temperature, pH, and concentration of SPB and SPFB, respectively. As a result, the changing material form and adding iron (III) oxide-hydroxide helped to improve material efficiency for RB4 dye adsorption than only changing material form.

Therefore, sawdust materials could be removed both lead and RB4 dye in aqueous solutions, and SPFB demonstrated the highest removal efficiency on both pollutants. Finally, SPFB was recommended to be applied for lead or RB4 dye removal in the wastewater treatment system in the future.

Adsorption isotherms for lead and RB4 dye adsorptions.

The adsorption patterns of sawdust powder (SP), sawdust powder doped iron (III) oxide-hydroxide (SPF), sawdust beads (SPB), and sawdust powder doped iron (III) oxide-hydroxide beads (SPFB) for lead adsorption and sawdust beads (SPB) and sawdust powder doped iron (III) oxide-hydroxide beads (SPFB) for RB4 dye adsorption were investigated through various adsorption isotherms of Langmuir, Freundlich, Temkin, and Dubinin–Radushkevich models in both linear and nonlinear models. For linear models, Langmuir, Freundlich, Temkin, and Dubinin–Radushkevich isotherms were plotted by C_e/q_e versus C_e, log q_e versus log C_e, q_e versus ln C_e, and ln q_e versus ε^2, respectively. For nonlinear models, all isotherms were plotted by C_e versus q_e. The plotting graphs of lead and RB4 dye adsorption demonstrated in Figs. 6a–h and 7a–f, respectively, and their isotherm parameters were illustrated in Tables 4 and 5, respectively. Generally, the best-fit isotherm model for explaining the adsorption pattern of material is chosen from the high regression value (R^2) which is close to 1[12].

For lead adsorption, the adsorption patterns of SP and SPB corresponded to Langmuir isotherm with relating to a physical adsorption because their R^2 values in both linear and nonlinear had higher than Freundlich, Temkin, and Dubinin–Radushkevich models. Therefore, Langmuir parameters of q_m and K_L values were used for explaining the adsorption pattern. Since q_m and K_L values of SPB were higher than SP, SPB had possibly higher lead removal efficiency with a high adsorption rate than SP correlated to the results of the batch experiment. For SPF and SPFB, their adsorption patterns corresponded to Freundlich isotherm with relating to a physiochemical adsorption because their R^2 values in both linear and nonlinear had higher than Langmuir, Temkin, and Dubinin–Radushkevich models. Therefore, Freundlich parameters of K_F and 1/n values were used for explaining the adsorption pattern. K_F refers Freundlich adsorption constant which SPFB represented the highest K_F value, so SPFB had a higher adsorption rate than SPF. For a 1/n value, it is a constant depiction of the adsorption intensity which 0 < 1/n < 1 means the favorable adsorption isotherm, so both materials were favorable adsorption since their 1/n values in this range.

For RB4 dye adsorption, the adsorption pattern of SPB corresponded to Langmuir model relating to a physical adsorption whereas the adsorption pattern of SPFB corresponded to the Freundlich model correlated to a physicochemical adsorption from choosing the highest R^2 value isotherm or closely to 1. These results corresponded to lead adsorption patterns that Langmuir and Freundlich isotherms were best-fitted models for explaining lead adsorption patterns of SPB and SPFB. Therefore, both lead and RB4 dye adsorption patterns of SPB and SPFB were physical and physicochemical adsorption processes, respectively.

Moreover, the results of both linear and nonlinear Langmuir, Freundlich, Temkin, and Dubinin–Radushkevich models of all sawdust materials were agreed with each other, so the plotting of both linear and nonlinear isotherm models were also recommended for correct data translations[42–44].

Finally, the comparison of the maximum adsorption capacity (q_m) value for lead and RB4 dye adsorptions by various adsorbents is illustrated in Table 6. For the comparison of lead removal, all sawdust materials in this study had higher q_m values than q_m values from *Picea smithiana* sawdust, sawdust-based cellulose nanocrystals, lemon peels, pomelo peels, and onion peels. In addition, SPFB had a higher q_m value than all studies in Table 6 except the studies of Hajam et al. (Dibetou sawdust activated by HNO$_3$ and NaOH), Niu et al. (pine sawdust biochar modified with Mn-Zn ferrite), Aigbe and Kavaz (sawdust modified with zinc oxide), Liu et al. (sugarcane bagasse modified with Fe$_3$O$_4$), Zhao et al. (corncob biochar modified with CuFe$_2$O$_4$), Kang et al. (cassava stalks modified with Fe$_3$O$_4$), and Ahmadi et al. (melon peel). For the comparison of RB4 dye removal, both SPB and SPFB had higher q_m values than q_m values from bagasse, bagasse fly ash, and lemon peels demonstrated in Table 6.

Therefore, all sawdust materials in this study were highly efficient materials for lead and RB4 dye adsorptions, and they are potential materials for application in industrial applications in the future, especially SPFB.

Adsorption kinetics for lead and RB4 dye adsorptions. The adsorption rates and mechanisms of lead adsorption by sawdust powder (SP), sawdust powder doped iron (III) oxide-hydroxide (SPF), sawdust beads (SPB), and sawdust powder doped iron (III) oxide-hydroxide beads (SPFB) and RB4 dye adsorption by sawdust beads (SPB) and sawdust powder doped iron (III) oxide-hydroxide beads (SPFB) were investigated through various the adsorption kinetics of pseudo-first-order kinetic model, pseudo-second-order kinetic model, Elovich model, and intraparticle diffusion in both linear and nonlinear models. For linear models, they were plotted by $\ln (q_e - q_t)$ versus time (t), t/q_t versus time (t), q_t versus $\ln t$, and q_t versus time ($t^{0.5}$) for pseudo-first-order kinetic, pseudo-second-order kinetic, Elovich, and intraparticle diffusion models, respectively. For nonlinear models, they were plotted by q_t versus time (t). The plotting graphs of lead and RB4 dye adsorptions illustrated in Figs. 8a–h and 9a–f, respectively, and their adsorption kinetic parameters were demonstrated in Tables 7 and 8, respectively. Generally, the best-fit isotherm model for explaining the adsorption rate and mechanism of material is chosen from the high regression value (R^2) which is close to 1[12].

For lead adsorption, the adsorption rate and mechanism of sawdust materials corresponded to a pseudo-second-order kinetic model with relating to the chemisorption process because their R^2 values in both linear and nonlinear pseudo-second-order kinetic models were higher than pseudo-first-order kinetic, Elovich, and intraparticle diffusion models. Therefore, the adsorption kinetic parameters of q_e and k_2 were used for explaining the adsorption rate and mechanism. Their adsorption capacities (q_e) of a pseudo-second-order kinetic model were arranged in order from high to low of SPFB > SPF > SPB > SP correlated to the results of batch experiments and adsorption isotherm. For a k_2 value, it is the pseudo-second-order kinetic rate constant in which SPFB demonstrated the highest value than other adsorbents. As a result, SPFB had higher lead adsorption with a fast reaction than other materials.

For RB4 dye adsorption, the adsorption rate and mechanism of SPB and SPFB corresponded to a pseudo-second-order kinetic model similar to lead adsorption. In addition, q_e and k_2 values of SPFB had also higher than SPB, so SPFB had higher RB4 dye adsorption than SPB corresponding to lead adsorption of SPB and SPFB. Therefore, both lead and RB4 dye adsorption rates and mechanisms of SPB and SPFB were explained by a physicochemical adsorption process.

Finally, the results of both linear and nonlinear pseudo-first-order, pseudo-second-order kinetic, Elovich, and intraparticle diffusion models of all sawdust materials were consistent with each other, so the plotting graphs of both linear and nonlinear kinetic models were also recommended for protecting mistake data translations[42–44].

Desorption experiments for lead and RB4 dye adsorptions. The desorption experiments were used to investigate the feasibility of the reuse of sawdust powder (SP), sawdust powder doped iron (III) oxide-hydroxide (SPF), sawdust beads (SPB), and sawdust powder doped iron (III) oxide-hydroxide beads (SPFB) because this is a necessary point to estimate the cost and economic feasibility of industrial applications.

For Lead adsorption, SP, SPF, SPB, and SPFB for 5 cycles of adsorption–desorption were applied to confirm their abilities, and their results are illustrated in Fig. 10a. For SP, it could be reused in 5 cycles with high adsorption and desorption in ranges of 63.33–82.16% and 60.54–81.76%, respectively which adsorption and desorption were decreased by approximately 19% and 21%, respectively. For SPF, it also confirmed to be reusability in 5 cycles with high adsorption and desorption in ranges of 81.83–95.23% and 78.30–94.93%, respectively which adsorption and desorption were decreased by approximately 13% and 17%, respectively. For SPB, it could be reused in 5 cycles with high adsorption and desorption in ranges of 71.58–88.62% and 68.33–88.27%, respectively which adsorption and desorption were decreased by approximately 17% and 20%, respectively. For SPFB, it also confirmed to be reusability in 5 cycles with high adsorption and desorption in ranges of 89.45–100% and 86.33–99.75%, respectively which adsorption and desorption were decreased by approximately 11% and 13%, respectively. Therefore, sawdust materials are potential materials for lead adsorption with the reusability of more than 5 cycles by more than 63%, and they can be further applied to industrial applications.

For RB4 dye adsorption, SPB and SPFB for 5 cycles of adsorption–desorption were applied to confirm their abilities, and their results are illustrated in Fig. 10b. For SPB, it could be reused in 5 cycles with high adsorption and desorption in ranges of 72.45–87.84% and 69.36–88.09%, respectively which adsorption and desorption were decreased by approximately 15% and 19%, respectively. For SPFB, it also confirmed to be reusability in 5 cycles with high adsorption and desorption in ranges of 82.85–92.63% and 80.15–92.43%, respectively which adsorption and desorption were decreased by approximately 10% and 12%, respectively. Therefore, SPB and SPFB are potential materials for RB4 dye removal with the reusability of more than 5 cycles by more than 72%, and they can be applied to industrial applications in the future.

The possible mechanisms of lead and dye adsorptions by sawdust materials

The possible mechanisms of lead and RB4 dye adsorptions on sawdust materials are demonstrated in Fig. 11a,b. For lead adsorption, the cellulose, hemicellulose, pectin, lignin, a hydroxyl group (–OH), methyl groups (C–H), aromatic ring represented lignin (C=C), and alcohol and carboxylic acid of lignin and hemicellulose (C–H) were the main structure and chemical functions groups of sawdust materials. The carboxyl group (–COOH) was also demonstrated in sawdust beads (SPB and SPFB) by forming the complex compound between SP or SPF with sodium alginate. In addition, the complex compound between the surface of SPF or SPFB and iron (III) oxide-hydroxide was formed to be $SP \cdot Fe(OH)_3$ or $SPB \cdot Fe(OH)_3$ by a process of electron sharing with hydroxyl groups of sawdust. Therefore, the possible mechanism of lead adsorption by sawdust materials might occur from donating a proton (H^+) from carboxyl groups (–COOH) or hydroxyl groups (–OH) or $SP \cdot Fe(OH)_3$ or $SPB \cdot Fe(OH)_3$ of
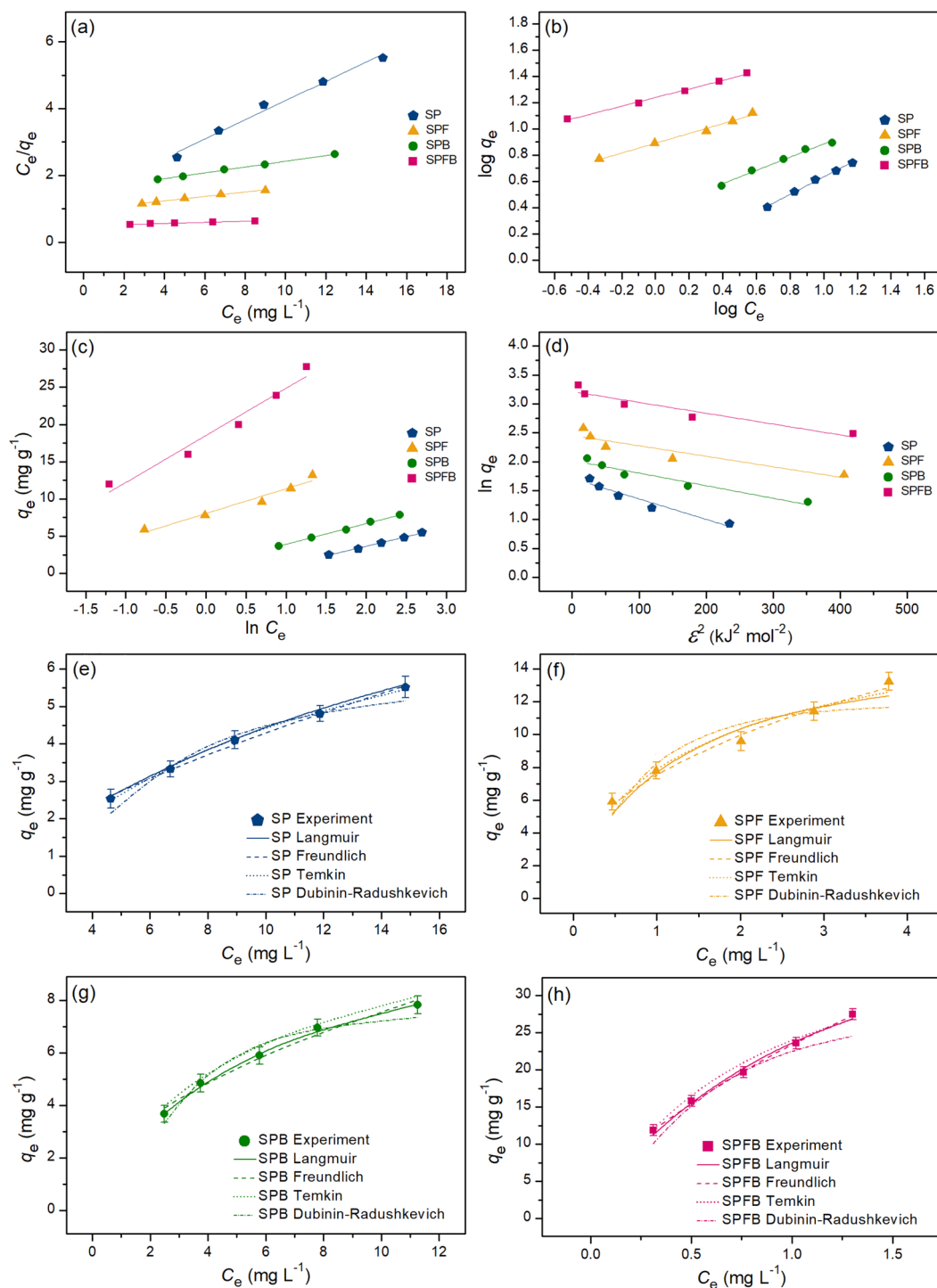
Figure 6. Graphs of (**a**) linear Langmuir, (**b**) linear Freundlich, (**c**) linear Temkin, (**d**) linear Dubinin–Radushkevich, and (**e–h**) nonlinear adsorption isotherms of sawdust powder (SP), sawdust powder doped iron (III) oxide-hydroxide (SPF), sawdust beads (SPB), and sawdust powder doped iron (III) oxide-hydroxide beads (SPFB) for lead adsorptions.

main chemical compounds or complex compounds to be $-COO$ or $-O$ or $FeO(OH)_2$ for capturing lead (II) ions (Pb^{2+}) by instead of H^+ from a process of electrostatic interactions[64] shown in Fig. 11a.

For RB4 dye adsorption, the main structure and chemical groups of SPB and SPFB were the same as mentioned above, but the possible mechanism of RB4 dye adsorption used a different explanation based on Ngamsurach et al.[12] shown in Fig. 11b. Three possible mechanisms of electrostatic attractions, hydrogen bonding interactions, and n−π bonding interactions were used for explaining RB4 dye adsorptions by SPB and SPFB. For
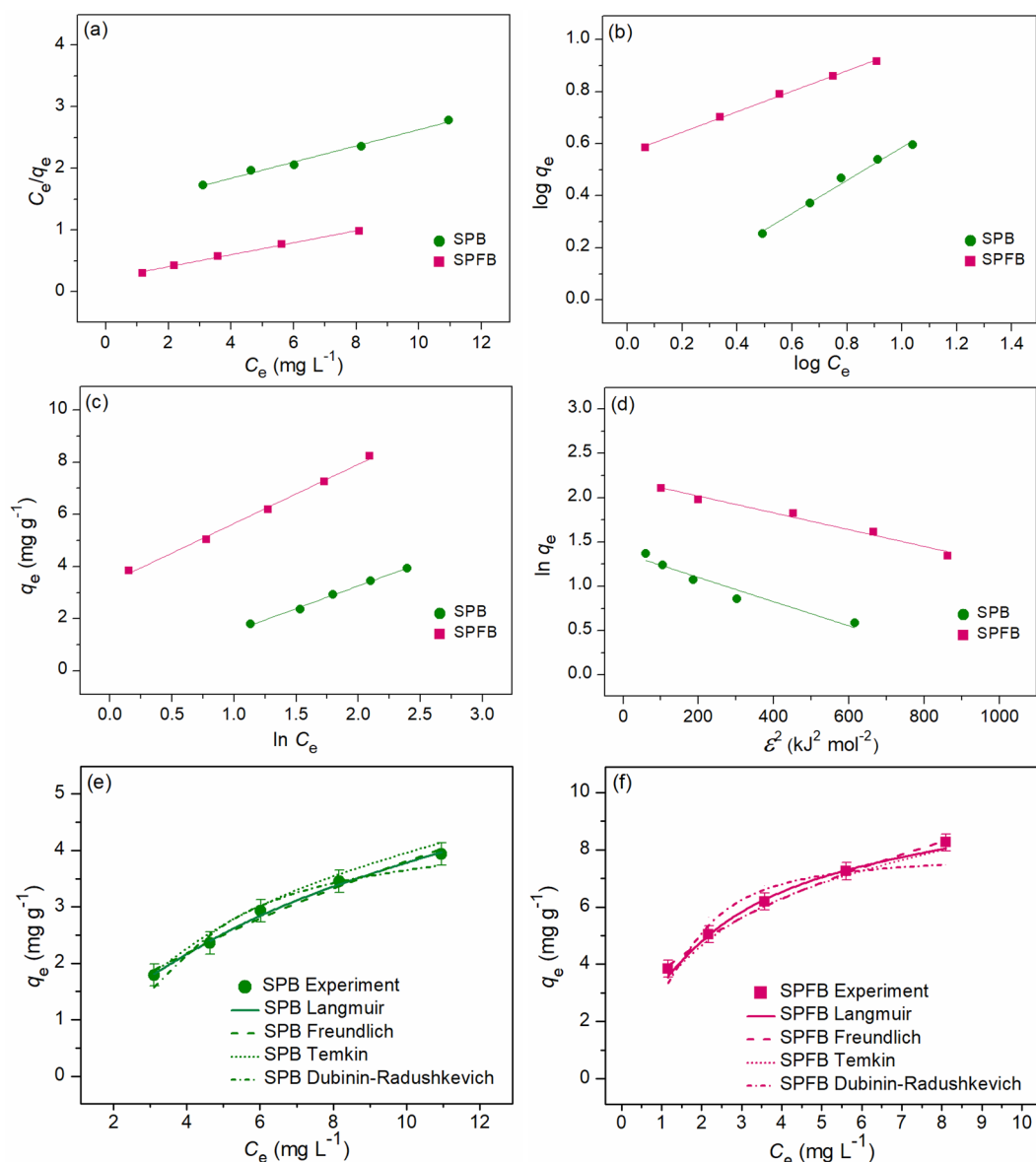
Figure 7. Graphs of (**a**) linear Langmuir, (**b**) linear Freundlich, (**c**) linear Temkin, (**d**) linear Dubinin–Radushkevich, and (**e,f**) nonlinear adsorption isotherms of sawdust beads (SPB), and sawdust powder doped iron (III) oxide-hydroxide beads (SPFB) for RB4 dye adsorptions.

electrostatic interactions, the surface of SPB or SPFB adsorbed RB4 dye molecule from the interaction between the positively charged hydroxy group (–OH) of their surface and the negatively charged sulfonate groups (–SO_3^-) of RB4 dye molecules. For hydrogen bonding interactions, the nitrogen (N) in the RB4 dye structure was caught by hydrogen ions (H^+) in the hydroxyl group (–OH) of SPB or SPFB[14]. Finally, the n–π bonding interactions occurred by the interaction of oxygen bond (–O) in the hydroxyl group (–OH) in SPB or SPFB and the aromatic rings in RB4 dye molecules[6].

Conclusion

Four sawdust materials of sawdust powder (SP), sawdust powder doped iron (III) oxide-hydroxide (SPF), sawdust beads (SPB), and sawdust powder doped iron (III) oxide-hydroxide beads (SPFB) were successfully synthesized for lead or RB4 dye removals in an aqueous solution. SPFB demonstrated higher specific surface area (11.020 m^2 g^{-1}) and smaller pore size (3.937 nm) than other materials, and the results illustrated that the addition of iron (III) oxide-hydroxide into sawdust materials increased the specific surface area and pore volume while the pore diameter size was decreased. The surface morphologies of SP and SPF were irregular shapes with heterogeneous fiber structures whereas SPB and SPFB had spherical shapes with coarse surfaces. Carbon (C) and oxygen (O) were found in all materials whereas iron (Fe) was only found in the materials with the addition of iron (III) oxide-hydroxide (SPF and SPFB). Four main function groups of O–H, C–H, C=C, and C–O were

Regression method	Isotherm model	Parameter	SP	SPF	SPB	SPFB
Linear	Langmuir	q_m (mg g^{-1})	11.737	15.924	12.771	47.170
		K_L (L mg^{-1})	0.059	0.992	0.155	1.014
		R^2	0.998	0.970	0.998	0.981
	Freundlich	$1/n$	0.666	0.372	0.503	0.128
		K_F (mg g^{-1}) (L mg^{-1})$^{1/n}$	0.930	7.773	2.411	11.495
		R^2	0.996	0.990	0.986	0.994
	Temkin	b_T (J mol^{-1})	970.639	745.622	750.520	1040.471
		A_T (L g^{-1})	0.566	11.297	1.414	24.249
		R^2	0.996	0.957	0.997	0.968
	Dubinin–Radushkevich	q_m (mg g^{-1})	5.537	11.678	7.547	24.863
		K_{DR} (mol^2 J^{-2})	0.004	0.009	0.001	0.003
		E (kJ mol^{-1})	11.952	7.454	21.320	12.910
		R^2	0.944	0.860	0.944	0.919
Nonlinear	Langmuir	q_m (mg g^{-1})	11.746	15.359	11.559	48.275
		K_L (L mg^{-1})	0.061	1.096	0.188	0.968
		R^2	0.999	0.973	0.999	0.990
		R^2_{adj}	0.998	0.964	0.999	0.987
		RMSE	0.121	0.879	0.096	0.701
	Freundlich	$1/n$	0.649	0.387	0.478	0.187
		K_F (mg g^{-1}) (L mg^{-1})$^{1/n}$	0.967	7.698	2.522	12.450
		R^2	0.997	0.993	0.988	0.999
		R^2_{adj}	0.995	0.990	0.984	0.999
		RMSE	0.080	0.389	0.227	0.229
	Temkin	b_T (J mol^{-1})	986.903	758.128	759.567	1033.791
		A_T (L g^{-1})	0.572	11.715	1.509	25.899
		R^2	0.996	0.958	0.997	0.971
		R^2_{adj}	0.994	0.945	0.996	0.962
		RMSE	0.091	0.708	0.098	1.220
	Dubinin–Radushkevich	q_m (mg g^{-1})	5.751	12.102	7.761	24.636
		K_{DR} (mol^2 J^{-2})	0.004	0.006	0.002	0.008
		E (kJ mol^{-1})	10.911	8.451	20.310	7.906
		R^2	0.937	0.863	0.936	0.917
		R^2_{adj}	0.916	0.818	0.914	0.889
		RMSE	0.342	1.384	0.485	2.051

Table 4. The comparison of linear and nonlinear isotherm parameters for lead adsorptions on sawdust powder (SP), sawdust powder doped iron (III) oxide-hydroxide (SPF), sawdust beads (SPB), and sawdust powder doped iron (III) oxide-hydroxide beads (SPFB).

detected in all materials. For batch experiments, the optimum conditions of SP, SPF, SPB, and SPFB for lead adsorptions were 2 g, 5 h, pH 5, 50 mg L^{-1}, 1 g, 3 h, pH 5, 50 mg L^{-1}, 1.5 g, 4 h, pH 5, 50 mg L^{-1}, and 0.5 g, 2 h, pH 5, 50 mg L^{-1}, respectively, and the optimum conditions of SPB and SPFB for RB4 dye adsorptions were 3 g, 12 h, 40 °C, pH 3, 50 mg L^{-1} and 1.5 g, 9 h, 30 °C, pH 3, 50 mg L^{-1}, respectively. Since SPFB demonstrated the highest lead or RB4 dye removal than other materials, adding iron (III) oxide-hydroxide and changing material form helped to improve material efficiencies for lead or RB4 dye adsorptions. For adsorption isotherms, SP and SPB corresponded to Langmuir model correlated to physical adsorption whereas SPF and SPFB corresponded to the Freundlich model relating to a physicochemical adsorption process. For the kinetic study, all materials corresponded to a pseudo-second-order kinetic model related to a chemisorption process with heterogenous adsorption. For desorption experiments, all materials could be reused more than 5 cycles with high lead removal of 63%, and SPB and SPFB also could be reused more than 5 cycles with high RB4 dye removal of 72%. Therefore, all sawdust materials were high potential materials for lead or dye adsorption in an aqueous solution, and SPFB demonstrated the highest lead and RB4 dye removals. Therefore, SPFB was suitable for wastewater treatment in industrial applications.

For future works, the real wastewater with contaminated lead or RB4 dye should be investigated to confirm the ability of sawdust materials, and the continuous flow study also needs to study for further industrial applications.

Materials and methods
Raw material. Sawdust (*Pterocarpus indicus*) was obtained from a local sawmill in Khon Kaen province, Thailand.

Regression method	Isotherm model	Parameter	SPB	SPFB
Linear	Langmuir	q_m (mg g^{-1})	7.605	10.309
		K_L (L mg^{-1})	0.100	0.455
		R^2	0.996	0.995
	Freundlich	$1/n$	0.635	0.394
		K_F (mg g^{-1}) (L mg^{-1})$^{1/n}$	0.895	1.418
		R^2	0.988	0.998
	Temkin	b_T (J mol^{-1})	398.331	407.163
		A_T (L g^{-1})	0.299	0.730
		R^2	0.954	0.985
	Dubinin–Radushkevich	q_m (mg g^{-1})	3.947	7.463
		K_{DR} (mol^2 J^{-2})	0.005	0.001
		E (kJ mol^{-1})	9.901	20.412
		R^2	0.945	0.967
Nonlinear	Langmuir	q_m (mg g^{-1})	7.536	10.161
		K_L (L mg^{-1})	0.102	0.470
		R^2	0.996	0.987
		R^2_{adj}	0.995	0.982
		RMSE	0.060	0.232
	Freundlich	$1/n$	0.603	0.385
		K_F (mg g^{-1}) (L mg^{-1})$^{1/n}$	0.950	1.722
		R^2	0.986	0.998
		R^2_{adj}	0.981	0.997
		RMSE	0.116	0.097
	Temkin	b_T (J mol^{-1})	396.218	410.654
		A_T (L g^{-1})	0.308	0.742
		R^2	0.956	0.986
		R^2_{adj}	0.942	0.981
		RMSE	0.205	0.238
	Dubinin–Radushkevich	q_m (mg g^{-1})	4.108	7.712
		K_{DR} (mol^2 J^{-2})	0.002	0.002
		E (kJ mol^{-1})	9.931	21.349
		R^2	0.948	0.969
		R^2_{adj}	0.931	0.959
		RMSE	0.224	0.714

Table 5. The comparison of linear and nonlinear isotherm parameters for RB4 dye adsorptions on sawdust beads (SPB) and sawdust powder doped iron (III) oxide-hydroxide beads (SPFB).

Chemicals. All chemicals were analytical grades (AR) without purification before use. For material synthesis, ferric chloride hexahydrate ($FeCl_3 \cdot 6H_2O$) (LOBA, India), sodium hydroxide (NaOH) (RCI Labscan, Thailand), sodium alginate ($NaC_6H_7O_6$) (Merck, Germany), and calcium chloride dehydrate ($CaCl_2 \cdot 2H_2O$) (RCI Labscan, Thailand) were used. For preparing wastewater samples, lead nitrate ($Pb(NO_3)_2$) (QRёC, New Zealand), and reactive blue 4 (RB4) dye (Sigma-Aldrich, Germany) were used. The chemical characteristic and structure of RB4 dye demonstrated in Table 9. For pH adjustment, 1% NaOH and 1% HNO_3 (Merck, Germany) were used.

Synthesis of four sawdust materials. The flow diagrams of synthesis methods of four sawdust materials which were sawdust powder (SP), sawdust powder doped iron (III) oxide-hydroxide (SPF), sawdust beads (SPB), and sawdust powder doped iron (III) oxide-hydroxide beads (SPFB) based on Threepanich and Praipipat[8] are demonstrated in Fig. 12a–c and the details were clearly explained below.

The synthesis of sawdust powder (SP). Firstly, sawdust was washed with tap water to remove contaminants, and then it was dried overnight in a hot air oven (Binder, FED 53, Germany) at 105 °C. Then, it was ground and sieved to a size of 125 μm. Finally, it was kept in a desiccator before use called sawdust powder (SP).

The synthesis of sawdust powder doped iron (III) oxide-hydroxide (SPF). Firstly, 5 g of SP were added to 500 mL of Erlenmeyer flask containing 160 mL of 5% $FeCl_3 \cdot 6H_2O$, and they were mixed by an orbital shaker (GFL, 3020, Germany) of 200 rpm for 3 h. Secondly, they were filtrated and air-dried at room temperature for 12 h. Then, they were added to 500 mL of Erlenmeyer flask containing 160 mL of 5% NaOH, and they were mixed by

Adsorbent materials	Dose	Contract time	Temperature (°C)	pH	Concentration (mg L^{-1})	q_m (mg g^{-1})	References
Lead adsorption							
Picea smithiana sawdust	20 g L^{-1}	1 h	25	8	0–200	8.53	[45]
Pinus halepensis sawdust	10 g L^{-1}	24 h	20–60	5–8	1–50	13.48	[46]
Dibetou sawdust	0.875 g	90 min		6	10–500	33.33	[37]
Dibetou sawdust activated by HNO$_3$ and NaOH	0.875 g	47.5 min	25	6	10–500	61.73	[37]
Sawdust based cellulose nanocrystals	5 mg L^{-1}		25–45	7	10–200	2.55	[47]
Sawdust biochar	0.1 g	24 h	25	6	10	17.57	[15]
Pine sawdust biochar modified with Mn–Zn ferrite	0.05 g	24 h	25	5	5–100	99.5	[48]
Sawdust modified with zinc oxide	0.05 g	100 min	25	8	100–600	92.59	[9]
Paddy husk biochar	0.1 g	24 h	25	6	10	14.20	[15]
Rice husk biochar	0.1 g			5–6	0–600	14.10–26.70	[49]
Coconut shells activated carbon doped Fe$_2$O$_3$	1.75 g L^{-1}	24 h	22	6	5–100	11.90	[50]
Macadamia nutshells modified Cu–Mn	0.1 g	2 h	25–45	6	100	34.50	[51]
Pineapple stem	0.05 g	5 h	25	5	50–150	13.30	[52]
Pineapple stem modified oxalic acid	0.05 g	5 h	25	5	50–150	27.70	[52]
Plum fruit biomass	0.2 g	30 min	22	6	5–300	28.80	[53]
Apricot kernels fruit biomass	0.2 g	30 min	22	6	5–300	23.90	[53]
Bagasse	1 g	2 h	–	5.5	40–240	31.45	[17]
Sugarcane bagasse modified with Fe$_3$O$_4$	50 mg	4 h	25–55	7	10–500	116.7	[10]
Corncob biochar modified with CuFe$_2$O$_4$	20 mg	8 h	30–50	5	60–500	132.10–134.41	[54]
Cassava stalks modified with Fe$_3$O$_4$	2 g	1 h	45	6	50–400	163.93	[55]
Watermelon seed	0.5 g	6 h	28–60	2	20–200	18.55–19.42	[56]
Lemon peel powder	4 g	6 h	25	5	10–70	1.81	[18]
Lemon peel with iron (III) oxide-hydroxide powder	3 g	6 h	25	5	10–70	3.52	[8]
Lemon peel beads	5 g	6 h	25	5	10–70	3.16	[18]
Lemon peel with iron (III) oxide-hydroxide beads	2 g	5 h	25	5	10–70	5.67	[8]
Orange peels	0.5 g	2 h		5	10–100	40.05	[57]
Pomelo peels		3 h	30	2.5	10–30	2.14	[58]
Banana peels	0.5 g	2 h		5	10–100	37.69	[59]
Melon peels	1.5 g L^{-1}	1 h	30	7	10–500	191.93	[19]
Onion peels	0.5 g	3 h	25	4	10–100	4.878	[60]
Onion peels modified with thioglycolic acid	0.5 g	3 h	25	4	10–100	6.173	[60]
SP	2 g	5 h	25	5	30–70	11.74	This study
SPF	1 g	3 h	25	5	30–70	15.92	This study
SPB	1.5 g	4 h	25	5	30–70	12.77	This study
SPFB	0.5 g	2 h	25	5	30–70	47.17	This study
RB4 dye adsorption							
Ayous wood sawdust	0.03 g	2 h	25		10–1400	415.10	[61]
Husk of agarwood fruit hydrogel beads	0.03 g		30		200–600	156.25–270.27	[62]
Picea abies Karst.bark with ZnCl$_2$	1.5 g L^{-1}		22	4	30–1000	59.00	[63]
Picea abies Karst.bark with KOH	1.5 g L^{-1}		22	4	30–1000	339.15	[63]
Rice bran modified with SnO$_2$/Fe$_3$O$_4$	1.5 g	3 h	60	3	10–200	200.40–218.82	[11]
Bagasse beads	2 g	12 h	70	3	30–90	3.17	[12]
Bagasse beads with mixed iron (III) oxide-hydroxide	3 g	9 h	70	3	30–90	3.77	[12]
Bagasse beads with mixed zinc oxide	3 g	12 h	60	3	30–90	3.18	[12]
Bagasse fly ash beads	3 g	12 h	70	3	30–90	5.57	[12]
Bagasse fly ash beads with mixed iron (III) oxide-hydroxide	2 g	3 h	50	3	30–90	10.28	[12]
Bagasse fly ash with beads mixed zinc oxide	2 g	12 h	40	3	30–90	6.78	[12]
Chicken eggshell beads	0.4 g	12 h	50	3	30–90	24.10	[14]
Chicken eggshell beads mixed iron (III) oxide-hydroxide	0.3 g	12 h	50	3	30–90	30.49	[14]
Chicken eggshell beads mixed zinc oxide	0.4 g	12 h	50	3	30–90	20.41	[14]
Duck eggshell beads	0.4 g	12 h	50	3	30–90	12.63	[14]
Duck eggshell beads mixed iron (III) oxide-hydroxide	0.3 g	12 h	50	3	30–90	25.97	[14]
Duck eggshell beads mixed zinc oxide	0.4 g	12 h	50	3	30–90	19.23	[14]
Lemon peel beads-doped iron (III) oxide-hydroxide	3 g	6 h	30	3	30–90	3.23	[13]
Lemon peel beads-doped zinc oxide	3 g	9 h	30	3	30–90	2.59	[13]
Continued							

Adsorbent materials	Dose	Contract time	Temperature (°C)	pH	Concentration (mg L^{-1})	q_m (mg g^{-1})	References
SPB	3 g	12 h	40	3	30–70	7.61	This study
SPFB	1.5 g	9 h	30	3	30–70	10.31	This study

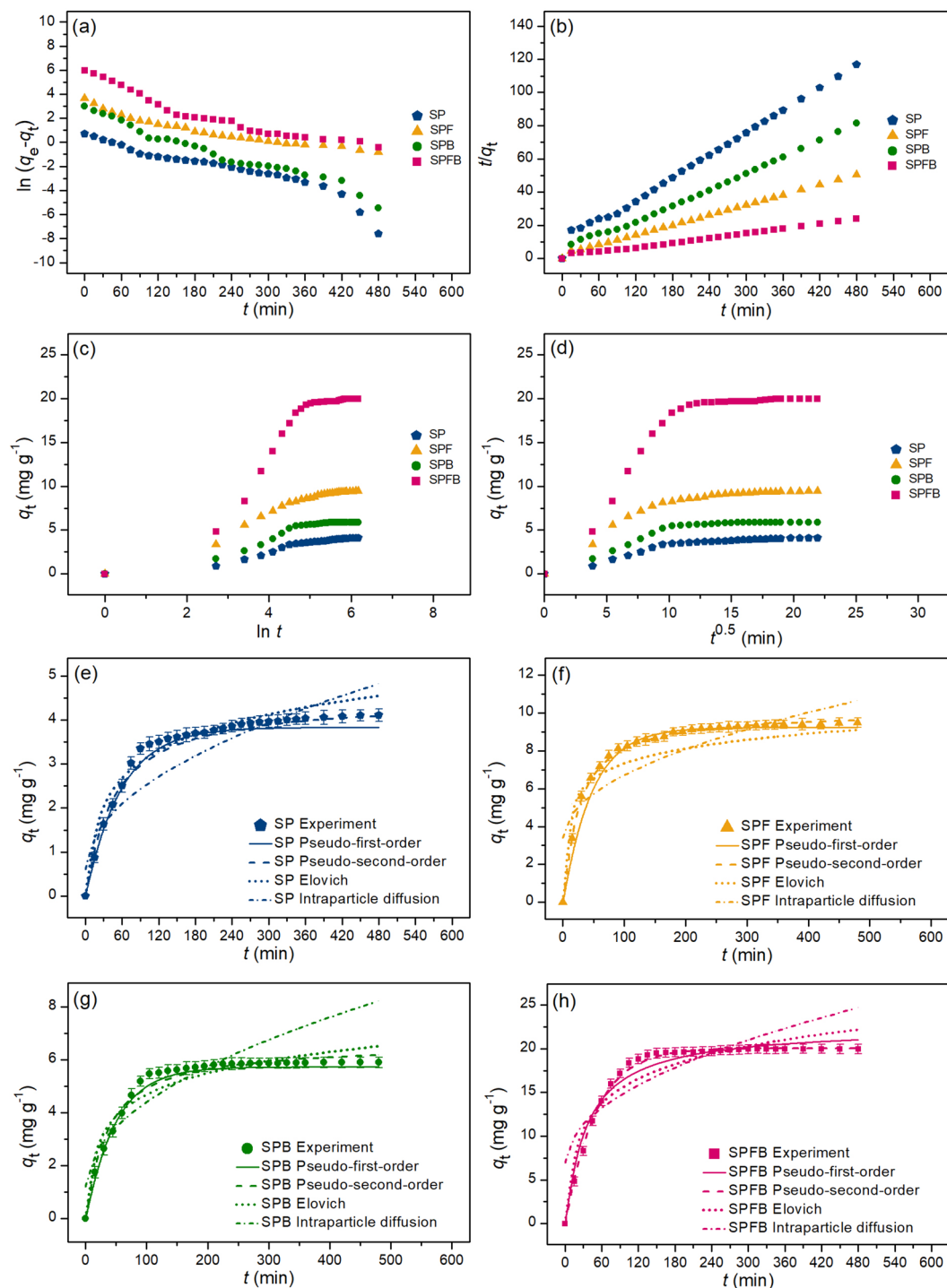**Table 6.** Comparison of the maximum adsorption capacity for lead and RB4 dye adsorptions by various adsorbents.

Figure 8. Graphs of (**a**) linear pseudo-first-order, (**b**) linear pseudo-second-order, (**c**) linear Elovich model (**d**) linear intraparticle diffusion, and (**e**–**h**) nonlinear kinetic models of sawdust powder (SP), sawdust powder doped iron (III) oxide-hydroxide (SPF), sawdust beads (SPB), and sawdust powder doped iron (III) oxide-hydroxide beads (SPFB) for lead adsorptions.
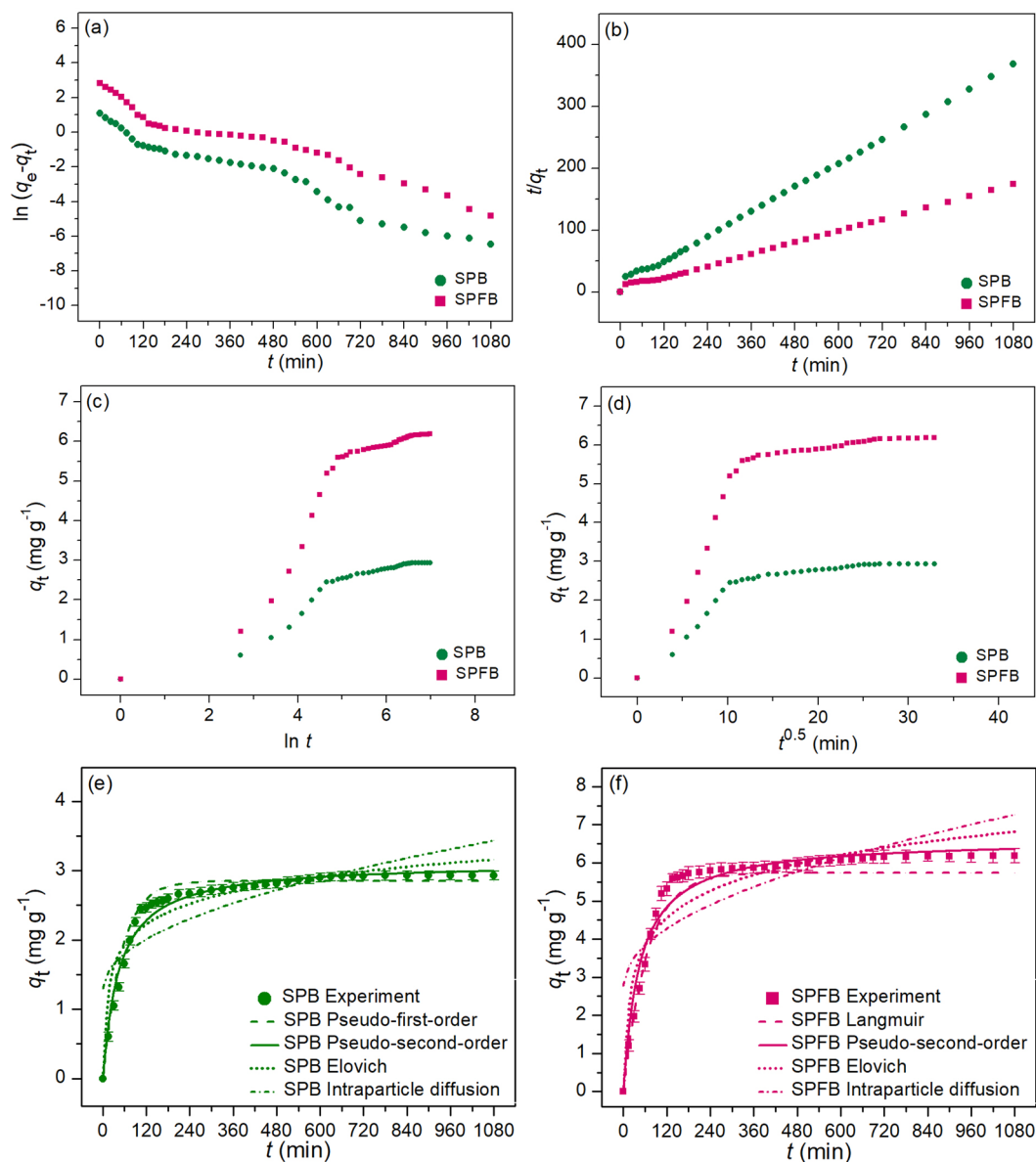
Figure 9. Graphs of (**a**) linear pseudo-first-order, (**b**) linear pseudo-second-order, (**c**) linear Elovich model (**d**) linear intraparticle diffusion, and (**e,f**) nonlinear kinetic models of sawdust beads (SPB) and sawdust powder doped iron (III) oxide-hydroxide beads (SPFB) for RB4 dye adsorptions.

an orbital shaker of 200 rpm for 1 h. After that, they were filtered and air-dried at room temperature for 12 h. Finally, they were kept in a desiccator before use called sawdust powder doped iron (III) oxide-hydroxide (SPF).

The synthesis of sawdust beads (SPB) or sawdust powder doped iron (III) oxide-hydroxide beads (SPFB). Firstly, 5 g of SP or SPF were added to 500 mL of a beaker containing 200 mL of 2% sodium alginate, and then they were homogeneously mixed and heated by a hot plate (Ingenieurbüro CAT, M. Zipperer GmbH, M 6, Germany) at 60 °C with a constant stirring of 200 rpm. Secondly, they were dropped by drop by using a 10 mL syringe with a needle size of 1.2×40 mm into 250 mL of 0.1 M $CaCl_2 \cdot 2H_2O$. The beaded samples were soaked in 0.1 M $CaCl_2 \cdot 2H_2O$ for 24 h, and then they were filtered and rinsed with DI water. After that, they were air-dried at room temperature for 12 h and kept in a desiccator before use called sawdust beads (SPB) or sawdust powder doped iron (III) oxide-hydroxide beads (SPFB).

Characterizations of sawdust materials. Various characterized techniques of Brunauer–Emmett–Teller (BET) (Bel, Bel Sorp mini X, Japan) by isothermal nitrogen gas (N_2) adsorption–desorption at 77.3 K and degas temperature of 80 °C for 6 h, field emission scanning electron microscopy and focus ion beam (FESEM-FIB) with energy dispersive X-ray spectrometer (EDX) (FEI, Helios NanoLab G3 CX, USA), and Fourier transform infrared spectroscopy (FT-IR) (Bruker, TENSOR27, Hong Kong) were used for investigating the specific

Regression method	Kinetic model	Parameter	SP	SPF	SPB	SPFB
Linear	Pseudo-first-order	q_e (mg g^{-1})	2.309	7.977	3.522	20.941
		k_1 (min^{-1})	0.010	0.019	0.018	0.022
		R^2	0.972	0.968	0.982	0.982
	Pseudo-second-order	q_e (mg g^{-1})	4.405	10.173	6.274	21.322
		k_2 (g mg^{-1} min^{-1})	0.004	0.012	0.007	0.047
		R^2	0.996	0.998	0.996	0.995
	Elovich	α (mg g^{-1} min^{-1})	5.477	6.465	5.944	7.327
		β (g mg^{-1})	1.646	0.440	0.863	0.267
		R^2	0.936	0.848	0.848	0.901
	Intraparticle diffusion	k_i (mg g^{-1} min$^{-0.5}$)	0.167	0.324	0.224	0.770
		C_i (mg g^{-1})	1.114	3.834	2.073	6.912
		R^2	0.803	0.721	0.720	0.705
Nonlinear	Pseudo-first-order	q_e (mg g^{-1})	2.376	8.036	3.724	20.963
		k_1 (min^{-1})	0.017	0.017	0.021	0.024
		R^2	0.974	0.970	0.984	0.984
		R^2_{adj}	0.973	0.969	0.983	0.983
		RMSE	0.167	0.369	0.189	1.297
	Pseudo-second-order	q_e (mg g^{-1})	4.486	10.231	6.305	22.578
		k_2 (g mg^{-1} min^{-1})	0.005	0.016	0.009	0.051
		R^2	0.994	0.997	0.997	0.996
		R^2_{adj}	0.993	0.997	0.996	0.995
		RMSE	0.157	0.119	0.498	0.939
	Elovich	α (mg g^{-1} min^{-1})	5.632	6.540	6.053	7.493
		β (g mg^{-1})	1.784	0.453	0.889	0.272
		R^2	0.939	0.851	0.851	0.906
		R^2_{adj}	0.937	0.845	0.846	0.902
		RMSE	0.256	0.823	0.821	1.572
	Intraparticle diffusion	k_i (mg g^{-1} min$^{-0.5}$)	0.173	0.331	0.237	0.811
		C_i (mg g^{-1})	1.134	3.917	2.176	6.964
		R^2	0.805	0.723	0.722	0.706
		R^2adj	0.798	0.713	0.712	0.699
		RMSE	0.458	1.122	1.124	2.310

Table 7. The comparison of linear and nonlinear kinetic parameters for lead adsorptions on sawdust powder (SP), sawdust powder doped iron (III) oxide-hydroxide (SPF), sawdust beads (SPB), and sawdust powder doped iron (III) oxide-hydroxide beads (SPFB).

surface area, pore volume, pore size, surface morphology, chemical compositions, and chemical functional groups of sawdust powder (SP), sawdust powder doped iron (III) oxide-hydroxide (SPF), sawdust beads (SPB), and sawdust powder doped iron (III) oxide-hydroxide beads (SPFB).

Batch adsorption experiments.   *Batch experiments for lead removal.*   A series of batch adsorption experiments were designed to investigate the effect of dose, contact time, pH, and concentration on lead removal efficiency by sawdust powder (SP), sawdust powder doped iron (III) oxide-hydroxide (SPF), sawdust beads (SPB), and sawdust powder doped iron (III) oxide-hydroxide beads (SPFB). The differences in dose from 0.5 to 3 g, contact time from 1 to 6 h, pH values of 1, 3, 5, 7, 9, 11, and lead concentration from 30 to 70 mg L^{-1} with the control condition of initial lead concentration of 50 mg L^{-1}, a sample volume of 200 mL, a shaking speed of 200 rpm, a temperature of 25 °C were applied. The lowest value of each affecting factor with the highest lead removal efficiency was selected as the optimum value, and that value was applied to the next affecting factor study. Lead concentrations were analyzed by an atomic adsorption spectrophotometer (PerkinElmer, PinAAcle 900 F, USA), and triplicate experiments were conducted to confirm the results. Lead removal in the percentage (%) to calculate the following Eq. (1).

$$\text{Lead removal efficiency (\%)} = (C_0 - C_e)/C_0 \times 100 \tag{1}$$

where C_0 is the initial lead concentration (mg L^{-1}), and C_e is the final lead concentration (mg L^{-1}).

Batch experiments for RB4 dye removal.   A series of batch adsorption experiments were designed to investigate the effect of dose, contact time, temperature, pH, and concentration on RB4 dye removal efficiency by sawdust beads (SPB) and sawdust powder doped iron (III) oxide-hydroxide beads (SPFB). The differences in dose from

Regression method	Kinetic model	Parameter	SPB	SPFB
Linear	Pseudo-first-order	q_e (mg g^{-1})	1.634	2.747
		k_1 (min^{-1})	0.006	0.007
		R^2	0.969	0.950
	Pseudo-second-order	q_e (mg g^{-1})	3.051	6.418
		k_2 (g mg^{-1} min^{-1})	0.005	0.009
		R^2	0.999	0.998
	Elovich	α (mg g^{-1} min^{-1})	0.783	0.872
		β (g mg^{-1})	2.128	1.223
		R^2	0.903	0.869
	Intraparticle diffusion	k_i (mg g^{-1} min$^{-0.5}$)	0.065	0.136
		C_i (mg g^{-1})	1.300	2.783
		R^2	0.653	0.613
Nonlinear	Pseudo-first-order	q_e (mg g^{-1})	1.713	2.873
		k_1 (min^{-1})	0.008	0.008
		R^2	0.973	0.951
		R^2_{adj}	0.972	0.949
		RMSE	0.142	0.339
	Pseudo-second-order	q_e (mg g^{-1})	3.117	6.623
		k_2 (g mg^{-1} min^{-1})	0.007	0.010
		R^2	0.995	0.996
		R^2_{adj}	0.994	0.995
		RMSE	0.105	0.305
	Elovich	α (mg g^{-1} min^{-1})	0.859	0.894
		β (g mg^{-1})	2.213	1.234
		R^2	0.904	0.871
		R^2_{adj}	0.901	0.867
		RMSE	0.229	0.550
	Intraparticle diffusion	k_i (mg g^{-1} min$^{-0.5}$)	0.073	0.155
		C_i (mg g^{-1})	1.331	3.057
		R^2	0.658	0.621
		R^2adj	0.649	0.610
		RMSE	0.415	0.950

Table 8. The comparison of linear and nonlinear kinetic parameters for RB4 dye adsorptions on sawdust beads (SPB) and sawdust powder doped iron (III) oxide-hydroxide beads (SPFB).

0.5 to 3 g, contact time of 3, 6, 9, 12, 15, 18 h, temperature from 30 to 80 °C, pH values of 1, 3, 5, 7, 9, 11, and RB4 dye concentration from 30 to 70 mg L^{-1} with the control condition of initial RB4 dye concentration of 50 mg L^{-1}, a sample volume of 200 mL, a shaking speed of 150 rpm, and a contact time of 12 h were applied. The lowest value of each affecting factor with the highest RB4 dye removal efficiency was selected as the optimum value, and that value was applied to the next affecting factor study. Dye concentrations were analyzed by UV–Vis spectrophotometer (Hitachi, UH5300, Japan) at a maximum wavelength of 595 nm, and triplicate experiments were conducted to confirm the results. Dye removal in the percentage (%) to calculate the following Eq. (2).

$$\text{Dye removal efficiency (\%)} = (C_0 - C_e)/C_0 \times 100 \tag{2}$$

where C_0 is the initial dye concentration (mg L^{-1}), and C_e is the final dye concentration (mg L^{-1}).

Adsorption isotherms. The adsorption patterns of sawdust powder (SP), sawdust powder doped iron (III) oxide-hydroxide (SPF), sawdust beads (SPB), and sawdust powder doped iron (III) oxide-hydroxide beads (SPFB) are investigated by adsorption isotherms for explaining that are the adsorption process of monolayer or multi-layer or heat or thermodynamic. Linear and nonlinear Langmuir, Freundlich, Temkin, and Dubinin–Radushkevich models are used to analyze followed Eqs. (3)–(10)[65–68].

Langmuir isotherm:

$$\text{Linear:} \quad C_e/q_e = 1/q_m K_L + C_e/q_m \tag{3}$$

$$\text{Nonlinear:} \quad q_e = q_m K_L C_e/1 + K_L C_e \tag{4}$$
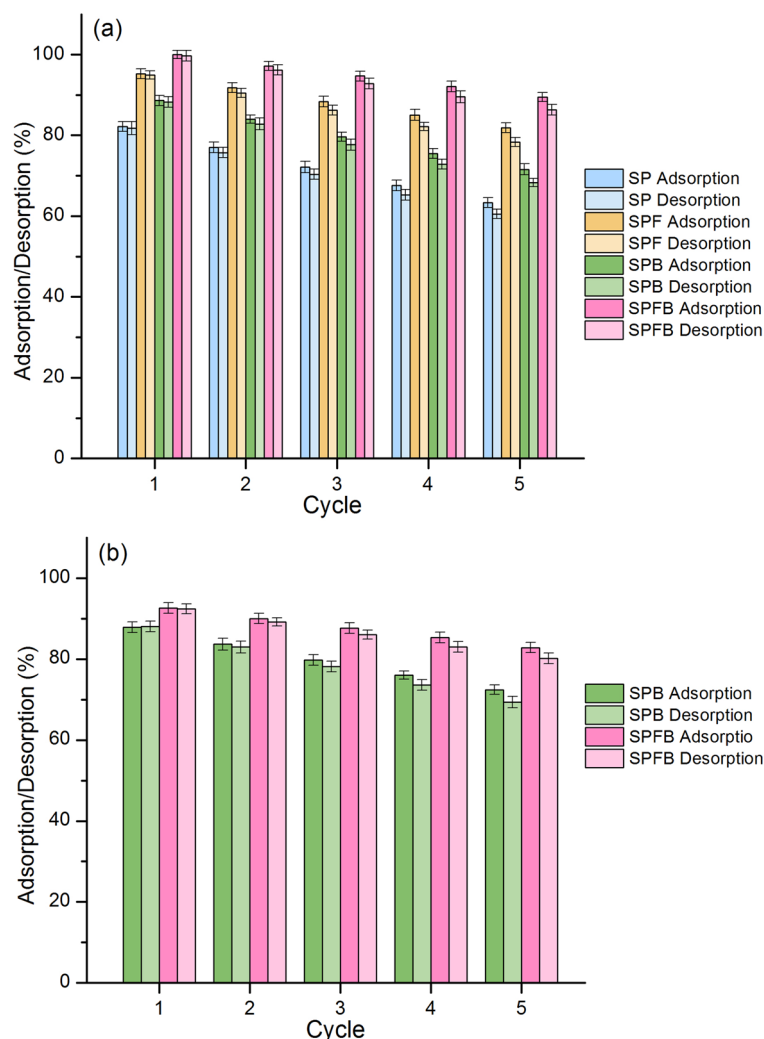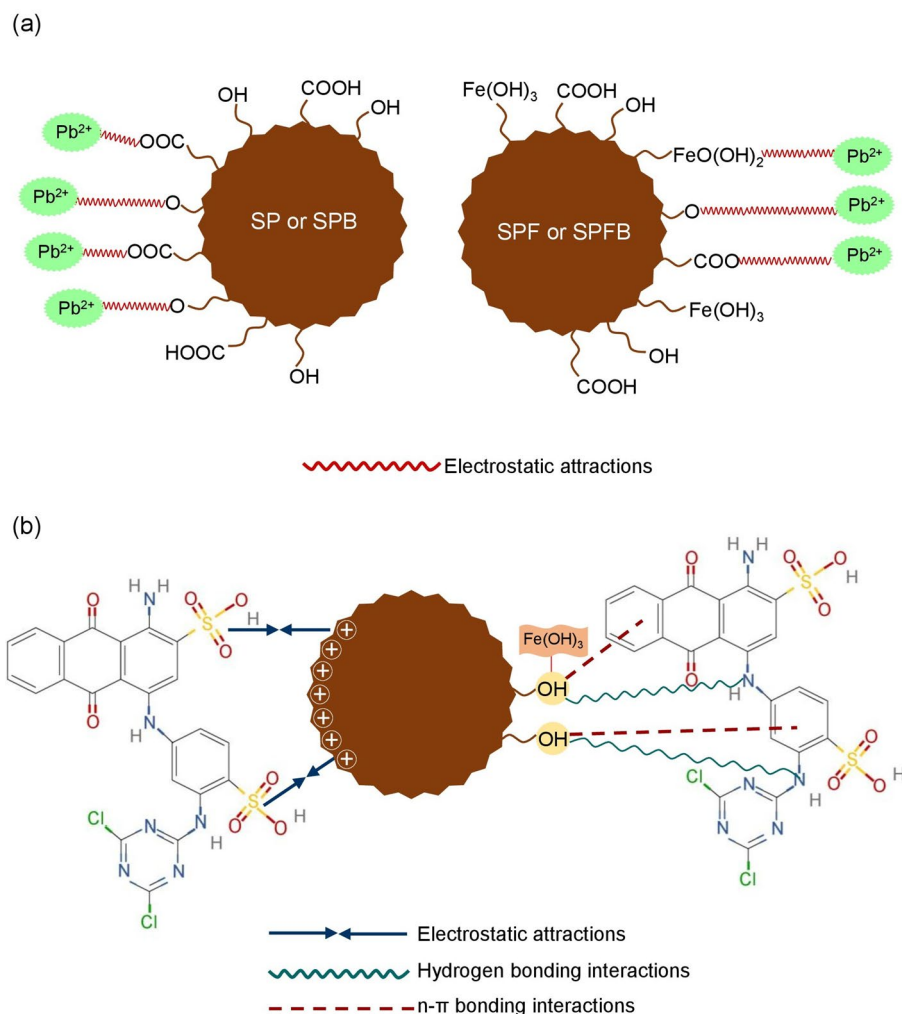
Freundlich isotherm:

Figure 10. The desorption experiments of (**a**) sawdust powder (SP), sawdust powder doped iron (III) oxide-hydroxide (SPF), sawdust beads (SPB), and sawdust powder doped iron (III) oxide-hydroxide beads (SPFB) for lead removal and (**b**) sawdust beads (SPB) and sawdust powder doped iron (III) oxide-hydroxide beads (SPFB) for RB4 dye removal.

$$\text{Linear:} \quad \log q_e = \log K_F + 1/n \log C_e \tag{5}$$

$$\text{Nonlinear:} \quad q_e = K_F C_e^{1/n} \tag{6}$$

Temkin isotherm:

$$\text{Linear:} \quad q_e = RT/b_T \ \ln A_T + RT/b_T \ \ln C_e \tag{7}$$

$$\text{Nonlinear:} \quad q_e = RT/b_T \ \ln A_T C_e \tag{8}$$

Dubinin–Radushkevich isotherm:

$$\text{Linear:} \quad \ln q_e = \ln q_m - K_{DR}\varepsilon^2 \tag{9}$$

$$\text{Nonlinear:} \quad q_e = q_m \exp(-K_{DR}\varepsilon^2) \tag{10}$$

where C_e is the equilibrium of lead or dye concentration (mg L^{-1}), q_e is the amount of adsorbed lead or dye on sawdust materials (mg g^{-1}), q_m is indicated as the maximum amount of lead or dye adsorption on adsorbent materials (mg g^{-1}), K_L is the adsorption constant (L mg^{-1}). K_F is the constant of adsorption capacity (mg g^{-1}) (L mg^{-1})$^{1/n}$, and $1/n$ is the constant depicting the adsorption intensity. R is the universal gas constant (8.314 J mol^{-1} K^{-1}), T is the absolute temperature (K), b_T is the constant related to the heat of adsorption (J mol^{-1}),

Figure 11. Possible mechanisms of (**a**) sawdust powder (SP), sawdust powder doped iron (III) oxide-hydroxide (SPF), sawdust beads (SPB), and sawdust powder doped iron (III) oxide-hydroxide beads (SPFB) for lead adsorption and (**b**) sawdust beads (SPB) and sawdust powder doped iron (III) oxide-hydroxide beads (SPFB) for RB4 dye adsorption.

and A_T is the equilibrium binding constant corresponding to the maximum binding energy (L g^{-1}). q_m is the theoretical saturation adsorption capacity (mg g^{-1}), K_{DR} is the activity coefficient related to mean adsorption energy (mol^2 J^{-2}), and ε is the Polanyi potential (J mol^{-1}). Graphs of linear Langmuir, Freundlich, Temkin, and Dubinin–Radushkevich isotherms were plotted by C_e/q_e versus C_e, log q_e versus log C_e, q_e versus ln C_e, and ln q_e versus ε^2, respectively whereas graphs of their nonlinear were plotted by q_e versus C_e.

For adsorption isotherm experiments, 2 g of SP or 1 g of SPF, or 1.5 g of SPB or 0.5 g of SPFB was added to 200 mL Erlenmeyer flasks with variable lead concentrations from 30 to 70 mg L^{-1} with the control condition of sample volume of 200 mL, a shaking speed of 200 rpm, pH 6, a temperature of 25 °C, and a contact time of 5 h for SP, 3 h for SPF, 4 h for SPB, and 2 h for SPFB for studying lead adsorption. For studying RB4 dye adsorption, 3 g of SPB or 1.5 g of SPFB was added to 200 mL Erlenmeyer flasks with variable RB4 dye concentrations from 30 to 70 mg L^{-1} with the control condition of a sample volume of 200 mL, a shaking speed of 150 rpm, pH 7, a temperature of 40 °C for SPB and 30 °C SPFB, and a contact time of 12 h.

Adsorption kinetics.   The adsorption mechanisms of sawdust powder (SP), sawdust powder doped iron (III) oxide-hydroxide (SPF), sawdust beads (SPB), and sawdust powder doped iron (III) oxide-hydroxide beads (SPFB) are determined by various adsorption kinetics which were linear and nonlinear pseudo-first-order kinetic, pseudo-second-order kinetic, Elovich, and intraparticle diffusion models calculated by Eqs. (11)–(17)[69–72].

Pseudo-first-order kinetic model:

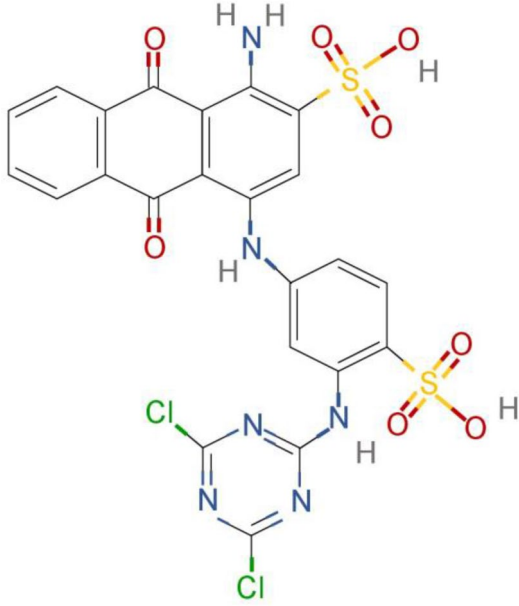$$\text{Linear:} \quad \ln (q_e - q_t) = \ln q_e - k_1 t \tag{11}$$

Properties and characteristics of dye	
Chemical structure	
Chemical name	Reactive blue 4 (RB4)
IUPAC name	1-amino-4-[3-[(4,6-dichloro-1,3,5-triazin-2-yl)amino]-4-sulfoanilino]-9,10-dioxoanthracene-2-sulfonic acid
Chemical formula	$C_{23}H_{14}Cl_2N_6O_8S_2$
Chemical class	Anionic dye
Molecular weight (g/mol)	637.43
(λ_{max}) (nm)	595
Color index number	61205

Table 9. The chemical characteristic and structure of RB4 dye.

$$\text{Nonlinear:} \quad q_t = q_e(1 - e^{-k_1 t}) \tag{12}$$

Pseudo-second-order kinetic model:

$$\text{Linear:} \quad t/q_t = 1/k_2 q_e^2 + (t/q_e) \tag{13}$$

$$\text{Nonlinear:} \quad q_t = k_2 q_e^2 t/(1 + q_e k_2 t) \tag{14}$$

Elovich model:

$$\text{Linear:} \quad q_t = 1/\beta \, \ln \, \alpha\beta + 1/\beta \, \ln \, t \tag{15}$$

$$\text{Nonlinear:} \quad q_t = \beta \, \ln \, t + \beta \, \ln \, \alpha \tag{16}$$

Intraparticle diffusion model:

$$\text{Linear and nonlinear:} \quad q_t = k_i t^{0.5} + C_i \tag{17}$$

where q_e is the amount of adsorbed lead or dye on adsorbent materials (mg g^{-1}), q_t is the amount of adsorbed lead or dye at the time (t) (mg g^{-1}), k_1 is a pseudo-first-order rate constant (min^{-1}), and k_2 is a pseudo-second-order rate constant (g mg^{-1} min^{-1})[73]. α is the initial adsorption rate (mg g^{-1} min^{-1}) and β is the extent of surface coverage (g mg^{-1}). k_i is the intraparticle diffusion rate constant (mg g^{-1} min$^{-0.5}$) and C_i is the constant that gives an idea about the thickness of the boundary layer (mg g^{-1}). Graphs of linear pseudo-first-order, pseudo-second-order, Elovich, and intraparticle diffusion models were plotted by ln ($q_e - q_t$) versus time (t), t/q_t versus time (t), q_t versus ln t, and q_t versus time ($t^{0.5}$), respectively whereas their nonlinear graphs were plotted by the capacity of lead or dye adsorbed by sawdust materials at the time (q_t) versus time (t).

For adsorption kinetic experiments, 10 g of SP or 5 g of SPF, or 7.5 g of SPB or 2.5 g of SPFB was added to 1000 mL of breaker with the control condition of the initial lead concentration of 50 mg L^{-1}, a sample volume of 1000 mL, a shaking speed of 200 rpm, pH 5, a temperature of 25 °C, and a contact time of 8 h for studying lead adsorption. For studying RB4 dye adsorption, 15 g of SPB or 7.5 g of SPFB was added to 1000 mL of breaker
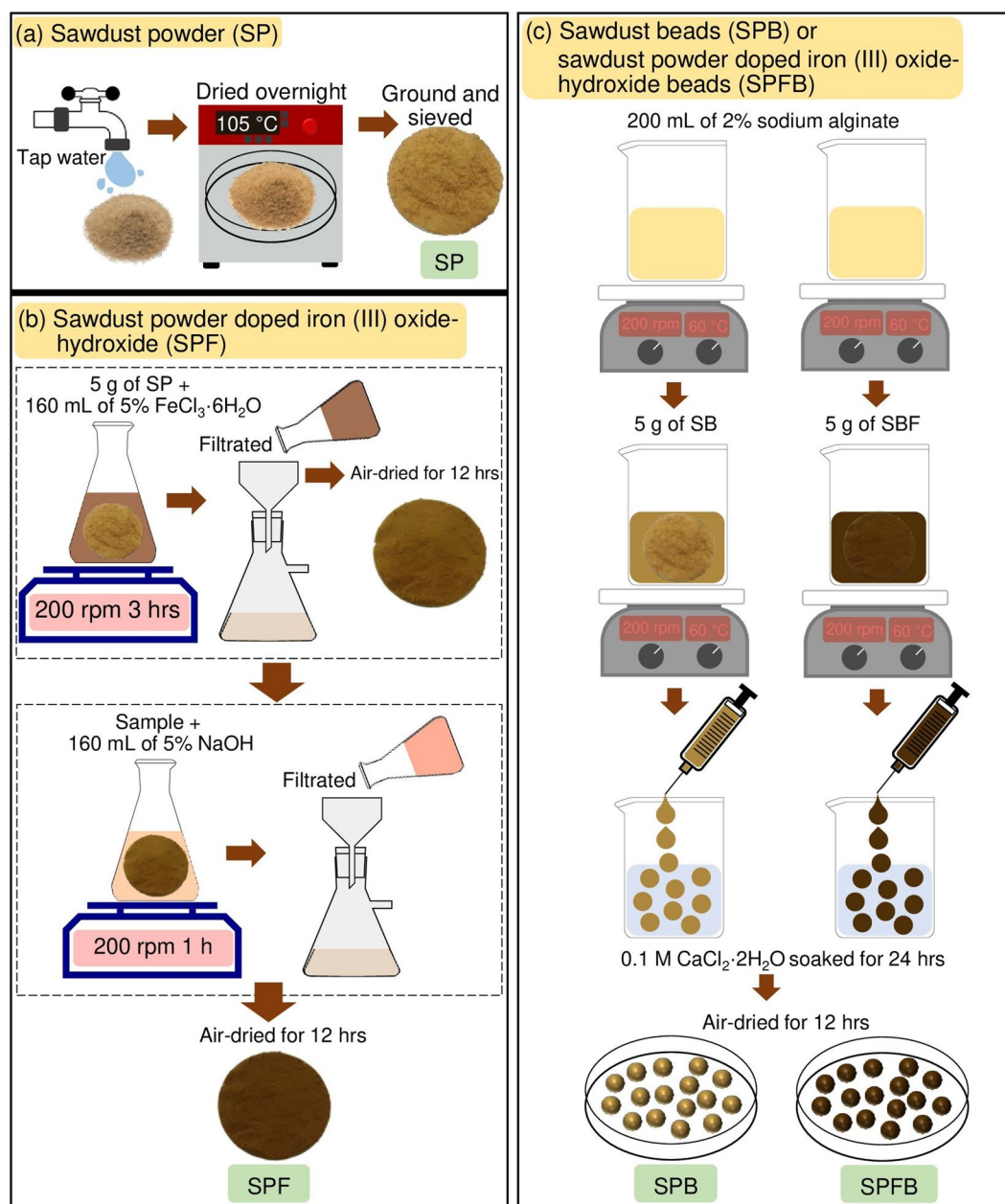
Figure 12. Flow diagrams of synthesis methods of (**a**) sawdust powder (SP), (**b**) sawdust powder doped iron (III) oxide-hydroxide (SPF), and (**c**) sawdust beads (SPB) and sawdust powder doped iron (III) oxide-hydroxide beads (SPFB).

with the control condition of initial RB4 dye concentration of 50 mg L^{-1}, a shaking speed of 150 rpm, pH 3, a temperature of 40 °C for SPB and 30 °C SPFB, and a contact time of 18 h.

Desorption experiments. The possible material reusability is an important factor for considering adsorbents of industrial applications, so the desorption experiments are designed to examine by studying five adsorption–desorption cycles to confirm the abilities of sawdust powder (SP), sawdust powder doped iron (III) oxide-hydroxide (SPF), sawdust beads (SPB), and sawdust powder doped iron (III) oxide-hydroxide beads (SPFB) for lead adsorption or sawdust beads (SPB) and sawdust powder doped iron (III) oxide-hydroxide beads (SPFB) for RB4 dye adsorption. For lead adsorption, the saturated sawdust materials were added to 500 mL of Erlenmeyer flask containing 200 mL of 0.5 M HNO₃ solution, then it was shaken by an incubator shaker (New Brunswick, Innova 42, USA) at 200 rpm for 6 h. Then, they were washed with deionization water and dried at room temperature, and sawdust materials are ready for the next adsorption cycle. For RB4 dye adsorption, the saturated sawdust materials were added to 500 mL of Erlenmeyer flask containing 200 mL of 0.01 M NaOH solution, then it was shaken by an incubator shaker at 150 rpm for 15 h with a temperature of 30 °C. Then, they were washed

with deionization water and dried at room temperature, and sawdust materials are ready for the next adsorption cycle. The desorption efficiency in percentage is calculated following Eq. (18).

$$\text{Desorption (\%)} = (q_d/q_a) \times 100 \tag{18}$$

where q_d is the amount of lead or dye desorbed (mg mL^{-1}) and q_a is the amount of lead or dye adsorbed (mg mL^{-1}).

Data availability

The datasets used and/or analyzed during the current study are available from the corresponding author upon reasonable request.

References

1. Tounsadi, H., Metarfi, Y., Taleb, M., El Rhazi, K. & Rais, Z. Impact of chemical substances used in textile industry on the employee's health: Epidemiological study. *Ecotoxicol. Environ. Saf.* **197**, 110594 (2020).
2. Li, M. *et al.* Review on clean recovery of discarded/spent lead-acid battery and trends of recycled products. *J. Power Sources* **436**, 226853 (2019).
3. Benkhaya, S., M'rabet, S. & El Harfi, A. A review on classifications, recent synthesis and applications of textile dyes. *Inorg. Chem. Commun.* **115**, 107891 (2020).
4. Al-Tohamy, R. *et al.* A critical review on the treatment of dye-containing wastewater: Ecotoxicological and health concerns of textile dyes and possible remediation approaches for environmental safety. *Ecotoxicol. Environ. Saf.* **231**, 113160 (2022).
5. Soliman, N. K. & Moustafa, A. F. Industrial solid waste for heavy metals adsorption features and challenges; A review. *J. Mater. Res. Technol.* **9**, 10235–10253 (2020).
6. Praipipat, P., Ngamsurach, P., Thanyahan, A. & Sakda, A. Reactive blue 4 adsorption efficiencies on bagasse and bagasse fly ash beads modified with titanium dioxide (TiO$_2$), magnesium oxide (MgO), and aluminum oxide (Al$_2$O$_3$). *Ind. Crops Prod.* **191**, 115928 (2023).
7. Ngamsurach, P., Namwongsa, N. & Praipipat, P. Synthesis of powdered and beaded chitosan materials modified with ZnO for removing lead (II) ions. *Sci. Rep.* **12**, 17184 (2022).
8. Threepanich, A. & Praipipat, P. Powdered and beaded lemon peels-doped iron (III) oxide-hydroxide materials for lead removal applications: Synthesis, characterizations, and lead adsorption studies. *J. Environ. Chem. Eng.* **9**, 106007 (2021).
9. Aigbe, R. & Kavaz, D. Unravel the potential of zinc oxide nanoparticle-carbonized sawdust matrix for removal of lead (II) ions from aqueous solution. *Chin. J. Chem. Eng.* **29**, 92–102 (2021).
10. Liu, G. *et al.* Organic adsorbents modified with citric acid and Fe$_3$O$_4$ enhance the removal of Cd and Pb in contaminated solutions. *Chem. Eng. J.* **395**, 125108 (2020).
11. Ma, C. M., Hong, G. B. & Wang, Y. K. Performance evaluation and optimization of dyes removal using rice bran-based magnetic composite adsorbent. *Materials (Basel)* **13**, 2764 (2020).
12. Ngamsurach, P., Nemkhuntod, S., Chanaphan, P. & Praipipat, P. Modified beaded materials from recycled wastes of bagasse and bagasse fly ash with iron (III) oxide-hydroxide and zinc oxide for the removal of reactive blue 4 dye in aqueous solution. *ACS Omega* **7**, 34839–34857 (2022).
13. Praipipat, P., Ngamsurach, P. & Prasongdee, V. Comparative reactive blue 4 dye removal by lemon peel bead doping with iron (III) oxide-hydroxide and zinc oxide. *ACS Omega* **7**, 41744–41758 (2022).
14. Praipipat, P., Ngamsurach, P., Saekrathok, C. & Phomtai, S. Chicken and duck eggshell beads modified with iron (III) oxide-hydroxide and zinc oxide for reactive blue 4 dye removal. *Arab. J. Chem.* **15**, 104291 (2022).
15. Wijeyawardana, P. *et al.* Removal of Cu, Pb and Zn from stormwater using an industrially manufactured sawdust and paddy husk derived biochar. *Environ. Technol. Innov.* **28**, 102640 (2022).
16. Hashem, A. *et al.* Non-linear adsorption characteristics of modified pine wood sawdust optimised for adsorption of Cd(II) from aqueous systems. *J. Environ. Chem. Eng.* **8**, 103966 (2020).
17. Harripersadth, C., Musonge, P., Makarfi Isa, Y., Morales, M. G. & Sayago, A. The application of eggshells and sugarcane bagasse as potential biomaterials in the removal of heavy metals from aqueous solutions. *South Afr. J. Chem. Eng.* **34**, 142–150 (2020).
18. Threepanich, A. & Praipipat, P. Efficacy study of recycling materials by lemon peels as novel lead adsorbents with comparing of material form effects and possibility of continuous flow experiment. *Environ. Sci. Pollut. Res.* **29**, 46077–46090 (2022).
19. Ahmadi, H. *et al.* Low cost biosorbent (melon peel) for effective removal of Cu (II), Cd (II), and Pb (II) ions from aqueous solution. *Case Stud. Chem. Environ. Eng.* **6**, 100242 (2022).
20. Grassi, P. *et al.* Application of *Cordia trichotoma* sawdust as an effective biosorbent for removal of crystal violet from aqueous solution in batch system and fixed-bed column. *Environ. Sci. Pollut. Res.* **28**, 6771–6783 (2021).
21. Bouhadjra, K., Lemlikchi, W., Ferhati, A. & Mignard, S. Enhancing removal efficiency of anionic dye (Cibacron blue) using waste potato peels powder. *Sci. Rep.* **11**, 2090 (2021).
22. Munagapati, V. S., Yarramuthi, V., Kim, Y., Lee, K. M. & Kim, D. S. Removal of anionic dyes (Reactive Black 5 and Congo Red) from aqueous solutions using Banana Peel Powder as an adsorbent. *Ecotoxicol. Environ. Saf.* **148**, 601–607 (2018).
23. Bayomie, O. S. *et al.* Novel approach for effective removal of methylene blue dye from water using fava bean peel waste. *Sci. Rep.* **10**, 7824 (2020).
24. Peyghami, A. *et al.* Evaluation of the efficiency of magnetized clinoptilolite zeolite with Fe$_3$O$_4$ nanoparticles on the removal of basic violet 16 (BV16) dye from aqueous solutions. *J. Dispers. Sci. Technol.* **1**, 1–10. https://doi.org/10.1080/01932691.2021.1947847 (2021).
25. Abdollahzadeh, H. *et al.* Efficiency of activated carbon prepared from scrap tires magnetized by Fe$_3$O$_4$ nanoparticles: Characterisation and its application for removal of reactive blue19 from aquatic solutions. *Int. J. Environ. Anal. Chem.* **102**, 1911–1925 (2022).
26. Rashtbari, Y. *et al.* Application of powdered activated carbon coated with zinc oxide nanoparticles prepared using a green synthesis in removal of reactive blue 19 and reactive black-5: Adsorption isotherm and kinetic models. *Desalin. Water Treat.* **179**, 354–367 (2020).
27. Pourali, P. *et al.* Removal of acid blue 113 from aqueous solutions using low-cost adsorbent: Adsorption isotherms, thermodynamics, kinetics and regeneration studies. *Sep. Sci. Technol.* **56**, 3079–3091 (2021).
28. Rashtbari, Y. *et al.* Green synthesis of zinc oxide nanoparticles loaded on activated carbon prepared from walnut peel extract for the removal of Eosin Y and Erythrosine B dyes from aqueous solution: Experimental approaches, kinetics models, and thermodynamic studies. *Environ. Sci. Pollut. Res.* **29**, 5194–5206 (2022).

29. Chen, X. *et al.* Natural adsorbent based on sawdust for removing impurities in waste lubricants. *J. Hazard. Mater.* **350**, 38–45 (2018).

30. Ibrahim, J. E. F. M., Tihtih, M. & Gömze, L. A. Environmentally-friendly ceramic bricks made from zeolite-poor rock and sawdust. *Constr. Build. Mater.* **297**, 123715 (2021).

31. Benyoucef, S. *et al.* Preparation and characterization of novel microstructure cellulosic sawdust material: Application as potential adsorbent for wastewater treatment. *Cellulose* **27**, 8169–8180 (2020).

32. Liang, J. *et al.* Magnetic nanoferromanganese oxides modified biochar derived from pine sawdust for adsorption of tetracycline hydrochloride. *Environ. Sci. Pollut. Res.* **26**, 5892–5903 (2019).

33. Pooladi, H., Foroutan, R. & Esmaeili, H. Synthesis of wheat bran sawdust/Fe_3O_4 composite for the removal of methylene blue and methyl violet. *Environ. Monit. Assess.* **193**, 276 (2021).

34. Houshangi, A., Jamehbozorgi, S., Yousefi, M. & Ghiasi, R. Preparation of $CoFe_2O_4$/sawdust and $NiFe_2O_4$/sawdust magnetic nano-composites for removal of oil from the water surface. *J. Chin. Chem. Soc.* **67**, 288–297 (2020).

35. Rouquerol, J. *et al.* Recommendations for the characterization of porous solids (Technical report). *Pure Appl. Chem.* **66**, 1739–1758 (1994).

36. Orelma, H., Tanaka, A., Vuoriluoto, M., Khakalo, A. & Korpela, A. Manufacture of all-wood sawdust-based particle board using ionic liquid-facilitated fusion process. *Wood Sci. Technol.* **55**, 331–349 (2021).

37. El Hajam, M. *et al.* Pb^{2+} ions adsorption onto raw and chemically activated Dibetou sawdust: Application of experimental designs. *J. King Saud Univ. Sci.* **32**, 2176–2189 (2020).

38. Zhong, C. *et al.* The role of sodium alginate in the flotation separation of apatite and dolomite. *Powder Technol.* **373**, 620–626 (2020).

39. Saeed, S. *et al.* La^{3+}-substituted β-ferrite: Investigation of structural, dielectric, FTIR and electrical polarization properties. *J. Alloys Compd.* **831**, 154854 (2020).

40. Rahman, N. U. *et al.* Activated *Ailanthus altissima* sawdust as adsorbent for removal of acid yellow 29 from wastewater: Kinetics approach. *Water* **13**, 2136 (2021).

41. Tejada-Tovar, C., Villabona-Ortíz, A., Ortega-Toro, R., Mancilla-Bonilla, H. & Espinoza-León, F. Potential use of residual sawdust of *Eucalyptus Globulus* Labill in Pb (II) adsorption: Modelling of the kinetics and equilibrium. *Appl. Sci.* **11**, 3125 (2021).

42. Ngamsurach, P. & Praipipat, P. Modified alginate beads with ethanol extraction of *Cratoxylum formosum* and *Polygonum odoratum* for antibacterial activities. *ACS Omega* **6**, 32215–32230 (2021).

43. Ngamsurach, P. & Praipipat, P. Antibacterial activities against *Staphylococcus aureus* and *Escherichia coli* of extracted *Piper betle* leaf materials by disc diffusion assay and batch experiments. *RSC Adv.* **12**, 26435–26454 (2022).

44. Ngamsurach, P. & Praipipat, P. Comparative antibacterial activities of *Garcinia cowa* and *Piper sarmentosum* extracts against *Staphylococcus aureus* and *Escherichia coli* with studying on disc diffusion assay, material characterizations, and batch experiments. *Heliyon* **8**, e11704 (2022).

45. Mahmood-Ul-Hassan, M., Yasin, M., Yousra, M., Ahmad, R. & Sarwar, S. Kinetics, isotherms, and thermodynamic studies of lead, chromium, and cadmium bio-adsorption from aqueous solution onto *Picea smithiana* sawdust. *Environ. Sci. Pollut. Res.* **25**, 12570–12578 (2018).

46. Semerjian, L. Removal of heavy metals (Cu, Pb) from aqueous solutions using pine (*Pinus halepensis*) sawdust: Equilibrium, kinetic, and thermodynamic studies. *Environ. Technol. Innov.* **12**, 91–103 (2018).

47. Oyewo, O. A., Ramaila, S., Mavuru, L., Leswifi, T. & Onyango, M. S. Adsorptive and coagulative removal of trace metals from water using surface modified sawdust-based cellulose nanocrystals. *J.* **4**, 193–205 (2021).

48. Niu, Z. *et al.* Green synthesis of a novel Mn–Zn ferrite/biochar composite from waste batteries and pine sawdust for Pb^{2+} removal. *Chemosphere* **252**, 126529 (2020).

49. Shi, J. *et al.* Removal of lead by rice husk biochars produced at different temperatures and implications for their environmental utilizations. *Chemosphere* **235**, 825–831 (2019).

50. Jaber, L. *et al.* Adsorptive removal of lead and chromate ions from water by using iron-doped granular activated carbon obtained from coconut shells. *Sustainability* **14**, 10877 (2022).

51. Morifi, E. L., Ofomaja, A. E. & Pillay, K. Microwave assisted modified macadamia nutshells/Cu–Mn oxide composite for the removal of Pb(II) from aqueous solution. *J. Environ. Chem. Eng.* **8**, 103822 (2020).

52. Vivian Loh, Z. T., Ping, T. Y. & Abdullah, A. H. Removal of Pb(II) from aqueous solution by pineapple plant stem. *Malays. J. Anal. Sci.* **23**, 219–228 (2019).

53. Pap, S. *et al.* Synthesis of highly-efficient functionalized biochars from fruit industry waste biomass for the removal of chromium and lead. *J. Mol. Liq.* **268**, 315–325 (2018).

54. Zhao, T., Ma, X., Cai, H., Ma, Z. & Liang, H. Study on the adsorption of $CuFe_2O_4$-loaded corncob biochar for Pb(II). *Molecules* **25**, 3456 (2020).

55. Kang, C. *et al.* EDTAD-modified cassava stalks loaded with Fe_3O_4: Highly efficient removal of Pb^{2+} and Zn^{2+} from aqueous solution. *Environ. Sci. Pollut. Res.* **28**, 6733–6745 (2021).

56. Adeoye, B. *et al.* Evaluation of biosorptive capacity of waste watermelon seed for lead (II) removal from aqueous solution. *Am. J. Environ. Eng.* **2020**, 1–8 (2020).

57. Afolabi, F. O., Musonge, P. & Bakare, B. F. Adsorption of copper and lead ions in a binary system onto orange peels: Optimization, equilibrium, and kinetic study. *Sustainability* **14**, 10860 (2022).

58. Yu, X. L. & He, Y. Optimal ranges of variables for an effective adsorption of lead(II) by the agricultural waste pomelo (*Citrus grandis*) peels using Doehlert designs. *Sci. Rep.* **8**, 729 (2018).

59. Afolabi, F. O., Musonge, P. & Bakare, B. F. Bio-sorption of a bi-solute system of copper and lead ions onto banana peels: Characterization and optimization. *J. Environ. Health Sci. Eng.* **19**, 613–624 (2021).

60. Olasehinde, E. F., Adegunloye, A. V., Adebayo, M. A. & Oshodi, A. A. Sequestration of aqueous lead(II) using modified and unmodified red onion skin. *Anal. Lett.* **51**, 2710–2732 (2018).

61. Teixeira, R. A. *et al.* Preparation of hybrids of wood sawdust with 3-aminopropyl-triethoxysilane. Application as an adsorbent to remove Reactive Blue 4 dye from wastewater effluents. *J. Taiwan Inst. Chem. Eng.* **125**, 141–152 (2021).

62. Ma, C. M., Yang, B. Y. & Hong, G. B. Husk of agarwood fruit-based hydrogel beads for adsorption of cationic and anionic dyes in aqueous solutions. *Molecules* **26**, 137 (2021).

63. Dos Reis, G. S. *et al.* Preparation and application of efficient biobased carbon adsorbents prepared from spruce bark residues for efficient removal of reactive dyes and colors from synthetic effluents. *Coatings* **11**, 772 (2021).

64. Malool, M. E., Keshavarz Moraveji, M. & Shayegan, J. Optimized production, Pb(II) adsorption and characterization of alkali modified hydrochar from sugarcane bagasse. *Sci. Rep.* **11**, 22328 (2021).

65. Langmuir, I. The adsorption of gases on plane surfaces of glass, mica and platinum. *J. Am. Chem. Soc.* **40**, 1361–1403 (1918).

66. Freundlich, H. Over the adsorption in solution. *J. Phys. Chem.* **57**, 385–470 (1906).

67. Temkin, M. I. & Pyzhev, V. Kinetics of ammonia synthesis on promoted iron catalysts. *Acta Physiochim. URSS* **12**, 327–356 (1940).

68. Dubinin, M. M. & Radushkevich, L. V. The equation of the characteristic curve of activated charcoal. *Proc. USSR Acad. Sci.* **55**, 327–329 (1947).

69. Lagergren, S. About the theory of so-called adsorption of soluble substances. *K. Sven. Vetenskapsakademiens Handl.* **24**, 1–39 (1898).

70. Ho, Y. S. & Mckay, G. Pseudo-second order model for sorption processes. *Process Biochem.* **34**, 451–465 (1999).
71. Elovich, S. Y. & Larinov, O. G. Theory of adsorption from solutions of non electrolytes on solid (I) equation adsorption from solutions and the analysis of its simplest form, (II) verification of the equation of adsorption isotherm from solutions. *Izv. Akad. Nauk. SSSR Otd. Khim. Nauk.* **2**, 209–216 (1962).
72. Weber, W. J. & Morris, J. C. Kinetics of adsorption carbon from solution. *J. Sanit. Eng. Div.* **89**, 31–60 (1963).
73. Jangkorn, S., Youngme, S. & Praipipat, P. Comparative lead adsorptions in synthetic wastewater by synthesized zeolite A of recycled industrial wastes from sugar factory and power plant. *Heliyon* **8**, e09323 (2022).

Acknowledgements

Author contributions

P.P.: Supervision, Conceptualization, Funding acquisition, Investigation, Methodology, Validation, Visualization, Writing—Original Draft, Writing—Review and Editing. P.N.: Visualization, Writing—Original Draft. S.K.: Investigation. J.M.: Investigation.

Competing interests

The authors declare no competing interests.

Additional information

Correspondence and requests for materials should be addressed to P.P.

Reprints and permissions information is available at www.nature.com/reprints.

Publisher's note Springer Nature remains neutral with regard to jurisdictional claims in published maps and institutional affiliations.